Bulk Parameterization of the Snow Field in a Cloud Model

YUH-LANG LIN[1], RICHARD D. FARLEY AND HAROLD D. ORVILLE

Institute of Atmospheric Sciences, South Dakota School of Mines and Technology, Rapid City 57701

(Manuscript received 1 December 1982, in final form 5 February 1983)

ABSTRACT

A two-dimensional, time-dependent cloud model has been used to simulate a moderate intensity thunderstorm for the High Plains region. Six forms of water substance (water vapor, cloud water, cloud ice, rain, snow and hail, i.e., graupel) are simulated. The model utilizes the "bulk water" microphysical parameterization technique to represent the precipitation fields which are all assumed to follow exponential size distribution functions. Autoconversion concepts are used to parameterize the collision-coalescence and collision-aggregation processes. Accretion processes involving the various forms of liquid and solid hydrometeors are simulated in this model. The transformation of cloud ice to snow through autoconversion (aggregation) and Bergeron processes and subsequent accretional growth or aggregation to form hail are simulated. Hail is also produced by various contact mechanisms and via probabilistic freezing of raindrops. Evaporation (sublimation) is considered for all precipitation particles outside the cloud. The melting of hail and snow are included in the model. Wet and dry growth of hail and shedding of rain from hail are simulated.

The simulations show that the inclusion of snow has improved the realism of the results compared to a model without snow. The formation of virga from cloud anvils is now modeled. Addition of the snow field has resulted in the inclusion of more diverse and physically sound mechanisms for initiating the hail field, yielding greater potential for distinguishing dominant embryo types characteristically different from warm- and cold-based clouds.

1. Introduction

The fact that ice particles play an important role in the formation of precipitation is firmly established, although details of ice formation and growth processes in clouds are poorly understood. Detailed knowledge of ice processes is complicated by the variety of nucleation mechanisms which may initiate the ice phase, the multitude of shapes and forms of the ice particles themselves, and the often complex nature of their motions. In attempting to bring order to the multiplicity of ice forms, several ice particle classification schemes have been proposed over the years; in general, ice particles may be grouped into four main classes: ice crystals, snow, graupel and hail. The snow, graupel and hail particles possess appreciable terminal velocities and thus fall relative to the air, and may be termed precipitating ice particles.

Nearly 50 years ago, Bergeron (1935) theorized that precipitation formation almost invariably required the presence of ice particles, except in special situations. This theory is based on the realization that water drops and ice crystals cannot coexist in equilibrium at subfreezing temperatures due to the fact that the saturation vapor pressure over ice is less than that over water (Wegener, 1911). Bergeron suggested that ice crystals in supercooled clouds grow by vapor diffusion at the expense of the supercooled water drops until either all of the water drops are consumed or all of the ice has fallen out of the supercooled regions of the cloud. Findeisen (1939) provided support to Bergeron's ideas and the theory has been referred to variously as the Bergeron, Bergeron-Findeisen, or Wegener-Bergeron-Findeisen process; in this paper, we shall use the term Bergeron process.

Observations at middle and high latitudes, beginning in the era of the Thunderstorm Project (Byers and Braham, 1949), have provided considerable support for the importance of ice processes to precipitation formation in summertime convective clouds. Additional supportive observational studies have included Kuettner (1950), Project Whitetop (Koenig, 1963; Braham, 1964), Dye *et al.* (1974) and Hallett *et al.* (1978), where the degree of sophistication in the observations has increased dramatically with time. These studies have established the role of capture mechanisms (riming) in the subsequent growth of ice particles after attaining certain size thresholds through diffusional growth. The riming size threshold varies with crystal habit (Hobbs, 1974) but, once attained, quickly dominates particle growth. The density of the rime deposit has been determined experimentally to be a function of temperature, water drop size and impact velocity (Macklin, 1962; Pflaum and Prup-

[1] Present affiliation: Graduate Student, Department of Geology and Geophysics, Yale University, New Haven, CT 06520.

pacher, 1979). An additional complicating factor involving ice processes is the possibility of ice particle multiplication within certain size and temperature regions (Mossop, 1978) which can greatly enhance the normally low ice concentrations at relatively warm subfreezing temperatures indicated by ice nuclei measurements (as in Fletcher, 1962).

The theoretical studies of Danielsen *et al.* (1972) and Nelson (1979) have demonstrated the importance of ice particles in the development of precipitation. They used one-dimensional, detailed microphysical cloud models, including ice processes, and obtained results consistent with observations. Nelson's model appeared to be capable of detecting the dominant precipitation initiating mechanism and the dominant hailstone embryo type for various atmospheric situations. In a somewhat different approach, Koenig and Murray (1976) developed a two-dimensional, axisymmetric numerical cloud model with parameterized microphysics for water drops and ice particles. Interesting features of their approach include the calculation of the ice particle number concentration without specifying the form of the size distribution function, although the ice particles were assumed to be monodisperse for many of the physical processes and the use of variable ice particle density assumptions and, hence, different fallspeed relations, based on the mean particle mass and temperature. In that study, the general comparison of model simulation against observations was satisfactory, and the microphysical parameterizations seemed capable of capturing many of the observed properties of glaciating clouds with regard to the locations and sizes of the liquid and solid hydrometeors.

This study builds on a thesis by Chang (1977) and a paper by Orville and Kopp (1977). We modify the two-dimensional, slab-symmetric cloud model with bulk water microphysics described by Orville and Kopp (1977) by incorporating equations for snow originally developed and tested in a one-dimensional cloud model by Chang (1977). The primary results of Chang's study indicated the ability of the parameterized model to capture the dominant precipitation initiation mechanism and dominant hailstone embryo type for different soundings, similar to the results of Nelson's detailed model.

The following sections describe various aspects of the current study in greater detail. Section 2 examines the basic characteristics of snow and hail and provides some basic definitions used in this study. A general description of the cloud model and the parameterization scheme are given in Section 3, along with the various production terms, with particular attention devoted to the snow equations. Section 4 describes the initial and boundary conditions and the numerical techniques. The results of three comparative experiments to assess the influence of the inclusion of snow in the model are presented in Section 5. Section 6 provides further discussion of several points and presents conclusions from this study.

2. The properties of snow and hail

a. The properties of snow

We shall use the term snow rather loosely in this study to represent snow crystals, snowflakes and low-density graupel particles. According to the *Glossary of Meteorology,* snow is "precipitation composed of white or translucent ice crystals, chiefly in complex branched hexagonal form and often agglomerated into snowflakes." Snow particles typically range in size from 2 to 5 mm diameter with bulk densities ranging from 0.05 to 0.89 g cm^{-3} (Pruppacher and Klett, 1978). The major habits that snow crystals may assume are needles, plates, columns, dendrites and stellar crystals, with the particular habits being dependent on the temperature and supersaturation with respect to ice (Nakaya, 1954; Kobayashi, 1957; Magono and Lee, 1966; Mason, 1971).

Usually, ice crystals in a cloud grow by the diffusion of water vapor to their surface due to the Bergeron process (Byers, 1965) and can, under suitable conditions, increase in size to form snow crystals. Snow crystals may grow by deposition and also collect supercooled droplets that freeze on impact and endow the crystal with a rimed appearance (Mason, 1971). Snow crystals may also collide and aggregate to form snowflakes, this being more pronounced in ice supersaturation conditions (Hosler *et al.*, 1957; Hosler and Hallgren, 1961; Hobbs, 1965). By continued depositional growth, aggregation, and the collection and freezing of supercooled droplets, the snow crystals and snowflakes may become embryos for graupel and hail. The growth rate of these snow crystals and aggregates is governed by the terminal velocities, collision and aggregation efficiencies, while the terminal velocity is a function of the mass and the dimension of the particle itself (Locatelli and Hobbs, 1974; Pruppacher and Klett, 1978). Generally, the terminal velocity of snow is between 0.5 and 3 m s^{-1}.

Measurements in clouds over the Cascade Mountains, Washington reported by Hobbs (1975) show that at temperatures between −4 and −25°C, the range of number concentration of ice and snow crystals varies little with temperature on the average, and that the concentration may reach values as high as 10^7 m^{-3}. This may be a reflection of the possibility that ice crystal multiplication similar to that proposed by Mossop (1978) is important in the clouds studied by Hobbs. The studies of Gunn and Marshall (1958) and Passarelli (1978) have indicated the size distribution of snowflakes is similar in form to the well known Marshall and Palmer (1948) raindrop size distribution (i.e., inverse exponential).

b. The properties of hail

In clouds with sufficiently strong updrafts, the riming of snow crystals, snowflakes and graupel particles may continue until hailstones are produced. According to the *Glossary of Meteorology,* hail is "precipitation in the form of balls or irregular lumps of ice." An individual unit of hail is called a hailstone which, by convention, has a diameter of 5 mm or more. Smaller ice particles of similar character are called graupel, ice pellets or frozen rain. In this study, we shall use the term hail rather loosely to represent high-density graupel, ice pellets, frozen rain and hailstones.

The bulk density of hailstones tends to vary radially from surface to core, with alternating concentric layers of lower and higher density. The density of such hailstone shells has been found to vary usually between 0.8 and 0.9 g cm^{-3} (Pruppacher and Klett, 1978). The terminal velocities of hailstones range from about 10 to 40 m s^{-1} or more. Auer (1972) has summarized measurements on the size distribution of hailstones and graupel particles. The concentration for graupel particles with diameters between 0.5 and 5 mm range between 10^3 and 1 m^{-3}, while large hailstones of diameters between 2.5 and 8 cm range in concentration from 10^{-6} to 10^{-2} m^{-3}. Auer proposed an inverse power law to describe the hail size distributions while others, such as Douglas (1960) and Federer and Waldvogel (1975), have proposed inverse exponential distributions.

Present studies indicate that hailstones may originate either as graupel or frozen drops (Knight and Knight, 1979). For warm-based clouds with cloud base temperature 15°C or higher, the frozen drops predominate in the formation of hailstones, while for cold-based clouds with cloud base temperature 5°C or lower, hailstones usually originate as graupel particles. List (1960) and Knight and Knight (1979) identified graupel particles as embryos for about 80% of the sampled hailstones which fell in Switzerland and Colorado, where the vast majority of cloud base temperatures are 10°C or colder. The graupel embryos, in turn, may have originated as snow crystals or on small frozen drops. Therefore, snow is an important factor in hailstorms, especially for continental, cold-based clouds. Recent *in situ* observations support this point of view (Dye *et al.,* 1974; Gagin, 1971).

3. The cloud model

a. General description

This model is mainly based on Chang (1977) and Orville and Kopp (1977). It is a two-dimensional, time-dependent cloud model with bulk water microphysics. The domain of the model is 19.2 km in both the X and Z dimensions with a 200 m grid interval.

The model contains five classes of hydrometeors: cloud water, cloud ice, rain, snow and hail. Inclusion of the snow content field allows for an intermediate and distinct entity between the two forms of ice previously modeled, namely, the non-precipitating cloud ice field and the hail field, resulting in a more physically sound representation of ice in general and, in particular, in the production of hail. Previous versions of the model (e.g., Orville and Kopp, 1977) generated precipitating ice (hail) via either raindrop freezing or through a crude representation of the Bergeron process. The new treatment allows for more realistic hail generation mechanisms via the ice phase since the Bergeron process now produces snow which must undergo further growth before transforming to hail. In addition to the Bergeron process, snow may also be generated by contact freezing and aggregation of cloud ice. Hail may be produced by a variety of contact freezing mechanisms and via aggregation of snow. For the model warm-based clouds, the probability based freezing of raindrops (Bigg, 1953) is no longer the primary mechanism for producing hail embryos, since raindrop capture of cloud ice or snow can now be major hail generation mechanisms.

The microphysical equations for snow, as summarized below, generally follow the development of Chang (1977), although the two-dimensional, time-dependent (2DTD) version presented here differs from Chang's original treatment in some respects. The terminal velocity of rain now includes height dependency, and different values of parameters for the terminal velocity and density of snow are used. Chang's treatment did not include a Bergeron process, while previous versions of the 2DTD cloud model have simulated this process (e.g., Orville and Kopp, 1977). The 2DTD snow model includes the Bergeron process, but as a generation mechanism for snow instead of hail as originally developed. The approximation to the Bergeron process was also modified to conform to the more realistic scheme developed by Hsie *et al.* (1980), who also developed a modified form of the scheme to allow for coexistence of cloud water and cloud ice in the temperature region of −40 to 0°C. This scheme allows cloud ice to grow via deposition at the expense of cloud water which evaporates to water vapor (Bergeron process).

b. Cloud microphysics

The model contains five classes of hydrometeors, all treated in a highly parameterized fashion. The cloud water and cloud ice particles are assumed to be small enough that their terminal velocities can be neglected compared with the velocity of air, rain, snow and hail. The rain, snow and hail possess appreciable terminal velocities. The microphysical processes simulated in the model are demonstrated in Fig. 1 and explained in Table 1.

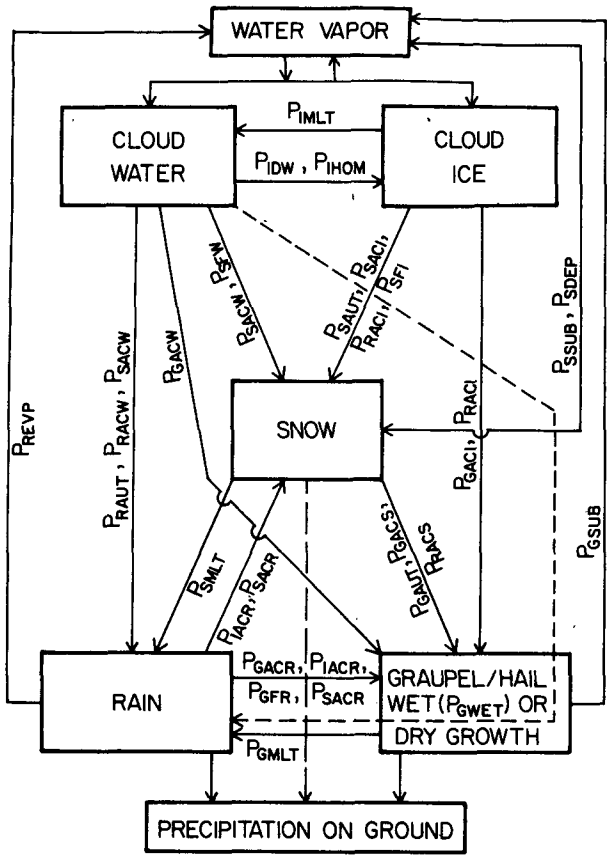

FIG. 1. Cloud physics processes simulated in the model with the snow field included. See Table 1 for an explanation of the symbols.

1) PARAMETERIZATION

Exponential size distributions are hypothesized for the precipitation particles:

$$n_R(D) = n_{0R} \exp(-\lambda_R D_R), \quad (1)$$

$$n_S(D) = n_{0S} \exp(-\lambda_S D_S), \quad (2)$$

$$n_G(D) = n_{0G} \exp(-\lambda_G D_G), \quad (3)$$

where n_{0R}, n_{0S} and n_{0G} are the intercept parameters of the rain, snow and hail size distributions, respectively. The n_{0R} is given by Marshall-Palmer (1948) as 8×10^{-2} cm^{-4}. According to the measurements of Gunn and Marshall (1958), n_{0S} is given as 3×10^{-2} cm^{-4}. Observations by Federer and Waldvogel (1975) of hail distributions lead to a value of $\sim 4 \times 10^{-4}$ cm^{-4} for n_{0G}. D_R, D_S and D_G are diameters of the rain, snow and hail particles, respectively. The slope parameters of the rain, snow and hail size distributions (λ_R, λ_S and λ_G, respectively) are determined by multiplying (1), (2) and (3) by particle mass and integrating over all diameters and equating the resulting quantities to the appropriate water contents; they may be written as

$$\lambda_R = \left(\frac{\pi \rho_W n_{0R}}{\rho l_R}\right)^{0.25}, \quad (4)$$

$$\lambda_S = \left(\frac{\pi \rho_S n_{0S}}{\rho l_S}\right)^{0.25}, \quad (5)$$

$$\lambda_G = \left(\frac{\pi \rho_G n_{0G}}{\rho l_G}\right)^{0.25}, \quad (6)$$

where l_W, l_S and l_G are densities of water, snow and hail, respectively. The density of snow is assumed to be 0.1 g cm^{-3} in this study. The symbols l_R, l_S and l_G are mixing ratios of rain, snow and hail, respectively.

The terminal velocities for a precipitating particle of diameter D_R, D_S or D_G are

TABLE 1. Key to Fig. 1

Symbol	Meaning
P_{IMLT}	Melting of cloud ice to form cloud water, $T \geq T_0$.
P_{IDW}	Depositional growth of cloud ice at expense of cloud water.
P_{IHOM}	Homogeneous freezing of cloud water to form cloud ice.
P_{IACR}	Accretion of rain by cloud ice; produces snow or graupel depending on the amount of rain.
P_{RACI}	Accretion of cloud ice by rain; produces snow or graupel depending on the amount of rain.
P_{RAUT}	Autoconversion of cloud water to form rain.
P_{RACW}	Accretion of cloud water by rain.
P_{REVP}	Evaporation of rain.
P_{RACS}	Accretion of snow by rain; produces graupel if rain or snow exceeds threshold and $T < T_0$.
P_{SACW}	Accretion of cloud water by snow; produces snow if $T < T_0$ or rain if $T \geq T_0$. Also enhances snow melting for $T \geq T_0$.
P_{SACR}	Accretion of rain by snow. For $T < T_0$, produces graupel if rain or snow exceeds threshold; if not, produces snow. For $T \geq T_0$, the accreted water enhances snow melting.
P_{SACI}	Accretion of cloud ice by snow.
P_{SAUT}	Autoconversion (aggregation) of cloud ice to form snow.
P_{SFW}	Bergeron process (deposition and riming)—transfer of cloud water to form snow.
P_{SFI}	Transfer rate of cloud ice to snow through growth of Bergeron process embryos.
P_{SDEP}	Depositional growth of snow.
P_{SSUB}	Sublimation of snow.
P_{SMLT}	Melting of snow to form rain, $T \geq T_0$.
P_{GAUT}	Autoconversion (aggregation) of snow to form graupel.
P_{GFR}	Probabilistic freezing of rain to form graupel.
P_{GACW}	Accretion of cloud water by graupel.
P_{GACI}	Accretion of cloud ice by graupel.
P_{GACR}	Accretion of rain by graupel.
P_{GACS}	Accretion of snow by graupel.
P_{GSUB}	Sublimation of graupel.
P_{GMLT}	Melting of graupel to form rain, $T \geq T_0$. (In this regime, P_{GACW} is assumed to be shed as rain.)
P_{GWET}	Wet growth of graupel; may involve P_{GACS} and P_{GACI} and must include P_{GACW} or P_{GACR}, or both. The amount of P_{GACW} which is not able to freeze is shed to rain.

$$U_{DR} = aD_R^b\left(\frac{\rho_0}{\rho}\right)^{1/2}, \quad (7)$$

$$U_{DS} = cD_S^d\left(\frac{\rho_0}{\rho}\right)^{1/2}, \quad (8)$$

$$U_{DG} = \left(\frac{4g\rho_G}{3C_D\rho}\right)^{1/2} D_G^{1/2}. \quad (9)$$

The terminal velocity U_{DR} of rain is suggested by Liu and Orville (1969) who performed a least squares analysis of Gunn and Kinzer's data (1949). The constants a and b are 2115 cm^{1-b} s^{-1} and 0.8, respectively. The terminal velocity U_{DS} of snow is based on the relations suggested by Locatelli and Hobbs (1974). Specifically, U_{DS} is that appropriate for graupel-like snow of hexagonal type, with the constants c and d being 152.93 cm^{1-d} s^{-1} and 0.25, respectively. The square root factor involving air density allows for increasing fallspeeds with increasing altitude, similar to Foote and du Toit (1969). The terminal velocity U_{DG} of hail is proposed by Wisner *et al.* (1972), with the drag coefficient C_D assumed to be 0.6.

Following Srivastava (1967), we define mass-weighted mean terminal velocities as

$$U = \int U_D l(D) dD / l, \quad (10)$$

where U_D is the terminal velocity of a precipitating particle of diameter D, $l(D)$ is the mixing ratio of a precipitating particle of diameter D, and l is the mixing ratio of a precipitating field. Applying (10) to each precipitating field, we obtain the mass-weighted mean terminal velocities of rain, snow and hail:

$$U_R = \frac{a\Gamma(4+b)}{6\lambda_R^b}\left(\frac{\rho_0}{\rho}\right)^{1/2}, \quad (11)$$

$$U_S = \frac{c\Gamma(4+d)}{6\lambda_S^d}\left(\frac{\rho_0}{\rho}\right)^{1/2}, \quad (12)$$

$$U_G = \frac{\Gamma(4,5)}{6\lambda_G^{0.5}}\left(\frac{4g\rho_G}{3C_D\rho}\right)^{1/2}. \quad (13)$$

The mass-weighted mean terminal velocities of rain, snow and hail are shown in Fig. 2.

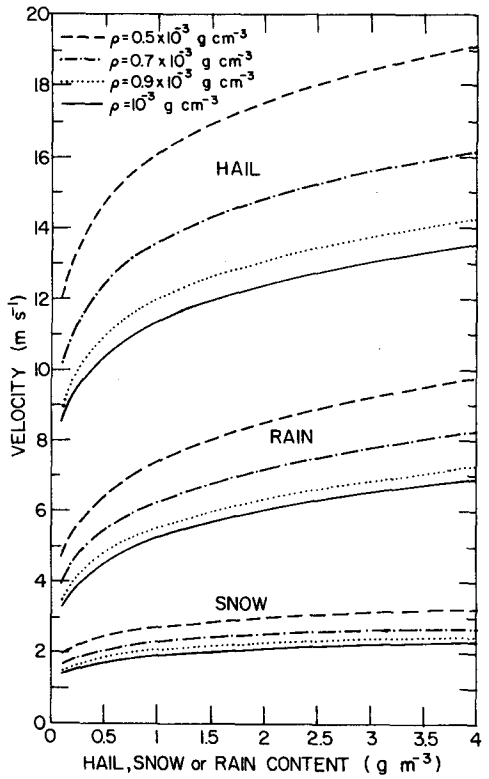

FIG. 2. Mass-weighted mean terminal velocities for rain, snow and hail. The four curves from 9 to 19 m s^{-1} are for hail. The four curves from 3 to 10 m s^{-1} are for rain. The remaining four curves are for snow.

2) WATER CONSERVATION EQUATIONS

Four conservation equations are considered here:

$$\frac{\partial q}{\partial t} = -\mathbf{V}\cdot\nabla q + \nabla\cdot K_h\nabla q - P_R - P_S - P_G, \quad (14)$$

$$\frac{\partial l_R}{\partial t} = -\mathbf{V}\cdot\nabla l_R + \nabla\cdot K_m\nabla l_R + P_R + \frac{1}{\rho}\frac{\partial}{\partial z}(U_R l_R \rho), \quad (15)$$

$$\frac{\partial l_S}{\partial t} = -\mathbf{V}\cdot\nabla l_S + \nabla\cdot K_m\nabla l_S + P_S + \frac{1}{\rho}\frac{\partial}{\partial z}(U_S l_S \rho), \quad (16)$$

$$\frac{\partial l_G}{\partial t} = -\mathbf{V}\cdot\nabla l_G + \nabla\cdot K_m\nabla l_G + P_G + \frac{1}{\rho}\frac{\partial}{\partial z}(U_G l_G \rho), \quad (17)$$

where $q = l_{CW} + l_{CI} + r$; l_{CW}, l_{CI}, l_R, l_S, l_G and r are the mixing ratios for cloud water, cloud ice, rain, snow, hail and water vapor, respectively; and P_R, P_S and P_G are the production terms for rain, snow and hail. These terms will be considered in more detail in the next several subsections. Only the final form of the microphysical equations will be presented here. For a more detailed explanation of the derivations, the reader is referred to Wisner *et al.* (1972) or Chang (1977).

The last terms in (15), (16) and (17) are the fallout terms. All of the first terms on the right-hand side are advection terms; the second terms are diffusion terms.

c. Production term for snow

We have noted earlier that ice crystals originally grow by deposition until reaching a size where aggregation and riming become important, leading to the formation of snow crystals and snowflakes. Within the model, the processes considered to generate snow are the collision and aggregation of the smaller cloud ice particles, contact freezing of small raindrops, and depositional growth and riming of ice crystals. Once generated, the snow continues to grow by accretion and deposition. Sublimation and melting reduce the snow content.

The total production term for snow may be written for two temperature regimes.

(i) If the temperature is below 0°C ($T < T_0$)

$$P_S = P_{SAUT} + P_{SACI} + P_{SACW} + P_{SFW} + P_{SFI} + P_{RACI}(\delta_3) + P_{IACR}(\delta_3) - P_{GACS} - P_{GAUT} - P_{RACS}(1 - \delta_2) + P_{SACR}(\delta_2) + P_{SSUR}(1 - \delta_1) + P_{SDEP}(\delta_1). \quad (18)$$

(ii) If the temperature is above 0°C ($T \geq T_0$)

$$P_S = P_{SMLT} - P_{GACS}, \quad (19)$$

where δ_1, δ_2 and δ_3 are defined as

$$\left.\begin{array}{l} T < T_0 \\ \quad \delta_1 = \begin{cases} 1, & \text{for } l_{CW} + l_{CI} > 0 \\ 0, & \text{otherwise} \end{cases} \\ \quad \delta_2 = \begin{cases} 1, & \text{for } l_R \text{ and } l_S < 10^{-4} \text{ g g}^{-1} \\ 0, & \text{otherwise} \end{cases} \\ \quad \delta_3 = \begin{cases} 1, & \text{for } l_R < 10^{-4} \text{ g g}^{-1} \\ 0, & \text{otherwise} \end{cases} \\ T \geq T_0 \\ \quad \delta_1 = \delta_2 = \delta_3 = 0 \end{array}\right\}. \quad (20)$$

Each production term will be discussed in detail below and typical values for most given later in Fig. 3.

1) Ice crystal aggregation

The aggregation rate of ice crystals to form snow is assumed to follow parameterization concepts originally proposed by Kessler (1969), to simulate the collision-coalescence process for cloud droplets. It may be written as

$$P_{SAUT} = \alpha_1(l_{CI} - l_{I0}), \quad (21)$$

where α_1 is a rate coefficient (s^{-1}), which is temperature dependent, and l_{I0} is a threshold amount for aggregation to occur. In this study, we set l_{I0} to be 10^{-3} g g^{-1}. The relationship used for the rate coefficient is

$$\alpha_1 = 10^{-3} \exp[0.025(T - T_0)],$$

which is a crude parameterization of the dependence of aggregation efficiency on crystal structure which, in turn, is temperature dependent.

The physically similar mechanism of aggregation of snow to form graupel, P_{GAUT}, will be described in subsection 3d, along with the other hail production terms.

2) Accretion

A variety of accretional growth mechanisms involving the interaction of snow with the other classes of hydrometeors are allowed in the model. There are also accretional processes involving the other classes of hydrometeors which may generate snow. The mathematical formulation for these accretional processes which produce or involve the snow content will now be described.

The accretion of cloud ice by snow is an aggregation process which occurs if the temperature is less than T_0 (273 K). The rate of accretional growth, P_{SACI}, is based on the geometric sweep-out concept integrated over all snow sizes for the assumed snow size distribution (2) which yields

$$P_{SACI} = \frac{\pi E_{SI} n_{0S} c l_{CI} \Gamma(3 + d)}{4\lambda_S^{3+d}} \left(\frac{\rho_0}{\rho}\right)^{1/2}, \quad (22)$$

where E_{SI} is the collection efficiency of the snow for cloud ice. Similar to the rate coefficient for ice crystal aggregation noted for (21), the collection efficiency of snow for cloud ice, E_{SI}, is assumed to be temperature dependent and can be expressed as

$$E_{SI} = \exp[0.025(T - T_0)]. \quad (23)$$

The accretion of cloud water by snow, P_{SACW}, is similar to (22), and is expressed as

$$P_{SACW} = \frac{\pi E_{SW} n_{0S} c l_{CW} \Gamma(3 + d)}{4\lambda_S^{3+d}} \left(\frac{\rho_0}{\rho}\right)^{1/2}, \quad (24)$$

where E_{SW} is the collection efficiency of snow for cloud water, which is assumed to be 1 in this model. P_{SACW} will increase the snow content by accreting the cloud water and subsequently freezing it if the temperature is lower than 0°C. If the temperature is warmer than 0°C, P_{SACW} will contribute to the rain content via the assumption that unfrozen water will be shed from the snow particles. This will be described later in subsection 3e. The sensible heat associated with the accreted cloud water will also enhance the melting of snow [see Eq. (32)].

In the following discussion, terminology which is largely an artifact of the hydrometeor classification scheme adapted for this study will be developed and applied. This artificiality is related to the various in-

teractions possible between liquid and solid water forms in the subfreezing regions. For the process of snow accreting cloud water, P_{SACW}, the interaction between the liquid (cloud water) and solid (snow) particles results in an increase in the original solid class (snow) and a loss in the accreted quantity (cloud water). We refer to this type of interaction as a *two-component* freezing process.

A more complicated situation is that typified by the interaction of rain and cloud ice. In this case, the interaction of small ice crystals (cloud ice) with large water drops (rain) produces a large ice particle (snow or hail). This situation in which the mutual interaction of two separate water classes (in this case, rain and cloud ice) results in a third, distinct water form (snow or hail in this case), is referred to as a *three-component* freezing process. For a three-component freezing process, two separate accretion rates must be calculated to determine the appropriate sink terms for each of the mutually interacting forms of water, and the sum of these two rates determines the source term for the distinct water form which results.

Having dispensed with these preliminary considerations, we now return to the microphysical development. In the temperature region $T < T_0$, supercooled water drops will freeze due to contact with solid particles. Accordingly, we assume that raindrops accreting cloud ice will freeze and the resultant solid particles contribute to the solid precipitation (snow or hail). Two production rates must be considered in this three-component freezing process; namely, the accretional rate of rain for cloud ice (P_{RACI}) and the freezing of raindrops which collide with cloud ice (P_{IACR}). The first rate is a sink for the cloud ice content, and the second is a sink for the rainwater content. Both terms are sources for either snow or hail, depending on the mass threshold criterion defined later in this section.

First, we consider the accretion of cloud ice by rain, a sink term for cloud ice and a source term for snow or hail. Applying the geometric sweep-out concept and integrating over all rain sizes for the assumed distribution given by (1), we obtain

$$P_{RACI} = \frac{\pi E_{RI} n_{0R} a l_{CI} \Gamma(3+b)}{4\lambda_R^{3+b}} \left(\frac{\rho_0}{\rho}\right)^{1/2}. \quad (25)$$

The collection efficiency of rain for cloud ice, E_{RI}, is assumed to be 1 in this model.

Now we shall consider the sink term for rain due to the presence of cloud ice, P_{IACR}, which is also a source term for snow or hail. Due to the lack of an individual prognostic value for cloud ice number concentration in the present model, we shall assume the small ice crystal size distribution to be monodisperse with each ice crystal being of constant mass $M_i = 4.19 \times 10^{-10}$ g. With raindrops and cloud ice particles assumed to be distributed evenly in the volume, and integrating over all raindrop sizes, we obtain the accretion rate of rain by cloud ice particles, P_{IACR}, which may be written as

$$P_{IACR} = \frac{\pi^2 E_{RI} n_{0R} a l_{CI} \rho_W \Gamma(6+b)}{24 M_i \lambda_R^{6+b}} \left(\frac{\rho_0}{\rho}\right)^{1.2}. \quad (26)$$

Since the cloud ice is small compared to raindrops, the density of the new product will be determined mainly by the amount of rain. In other words, the interaction of rain and cloud ice is likely to result in the formation of hailstones as long as the raindrops are fairly large. However, it is difficult to determine the result of each collision in this bulk water simulation; therefore, we will assign a threshold for the rainwater content to determine whether the interaction of rain and cloud ice results in snow or hail (see Fig. 1). Based on preliminary calculations, we concluded that if the mixing ratio of rain is $l_R < 10^{-4}$ g g^{-1}, then all the raindrops will be small enough to become low-density particles (snow). If $l_R > 10^{-4}$ g g^{-1}, then the P_{IACR} and P_{RACI} contribute to the formation of hail and provide an important collisional-freezing mechanism for the generation of frozen drop hailstone embryos. This collisional-freezing mechanism (three-component freezing) usually dominates over the probabilistic (Bigg, 1953) freezing of rain which had formerly been the sole avenue for the generation of frozen drop hailstone embryos.

We now consider the interaction between snowflakes and raindrops. The accretion rate of rain for snow, P_{RACS}, and the accretion rate of snow for rain, P_{SACR}, are as follows:

$$P_{RACS} = \pi^2 E_{SR} n_{0R} n_{0S} |U_R - U_S| \left(\frac{\rho_S}{\rho}\right) \times \left(\frac{5}{\lambda_S^6 \lambda_R} + \frac{2}{\lambda_S^5 \lambda_R^2} + \frac{0.5}{\lambda_S^4 \lambda_R^3}\right), \quad (27)$$

$$P_{SACR} = \pi^2 E_{SR} n_{0S} n_{0R} |U_S - U_R| \left(\frac{\rho_W}{\rho}\right) \times \left(\frac{5}{\lambda_R^6 \lambda_S} + \frac{2}{\lambda_R^5 \lambda_S^2} + \frac{0.5}{\lambda_R^4 \lambda_S^3}\right), \quad (28)$$

where the collection efficiency of snow (rain) for rain (snow), E_{SR}, is assumed to be 1. Derivation of (27) and (28) requires that we assume that all raindrops and snow particles are falling at their appropriate mass-weighted mean terminal velocities. The assumption is required due to the fact that the difference in fallspeeds of interacting particles must always be treated as a positive quantity to properly define the sweepout volume. This requirement is further complicated by the fact that the derivation of (27) and (28) requires a double integration over all raindrop and snow particle sizes.

A similar assumption is required in deriving other rates involving the collection of one class of precipitating particle by another class of precipitating particle, i.e., (29) and (42). Compared to detailed calculations in which the interacting species are discretized into many size categories, these four bulk rates may all provide erroneous estimates. The nature of the errors varies considerably over the full range of likely equivalent water content values and also is generally different for each rate. We have investigated various formulations of these bulk rates but have been unable as of yet to find satisfactory alternatives. We remain concerned with this problem, and efforts to remedy the erroneous estimates are continuing.

In the temperature region $T < T_0$, if $l_R \geq 10^{-4}$ g g^{-1} or $l_S \geq 10^{-4}$ g g^{-1}, we assume a three-component freezing process with both rates P_{SACR} and P_{RACS} contributing to the formation of hail. If the mass threshold criterion is not met, i.e., both l_R and l_S are less than 10^{-4} g g^{-1}, the physical interpretation changes to a two-component freezing process. In this case, the snow grows at the expense of the rain and only the rate P_{SACR} [Eq. (28)] need be calculated. In the temperature region $T \geq T_0$, P_{SACR} will not be active except to enhance the melting of the snow due to the sensible heat associated with the accreted rainwater [see Eq. (32)].

The accretion of snow by hail, P_{GACS}, always contributes to hail content whether the temperature is less than T_0 or not. The equation for the production rate is

$$P_{GACS} = \pi^2 E_{GS} n_{0S} n_{0G} |U_G - U_S| \left(\frac{\rho_S}{\rho}\right) \times \left(\frac{5}{\lambda_S^6 \lambda_G} + \frac{2}{\lambda_S^5 \lambda_G^2} + \frac{0.5}{\lambda_S^4 \lambda_G^3}\right), \quad (29)$$

where E_{GS}, the collection efficiency of hail particles for snow particles, is assumed to be a function of temperature given by

$$E_{GS} = \begin{cases} \exp[0.09(T - T_0)], & T < T_0 \\ 1.0, & T \geq T_0. \end{cases} \quad (30)$$

Note that the collection efficiency of hail for snow is considerably less than that of snow for ice crystals given by (23).

3) Deposition (sublimation)

The depositional growth rate of snow, P_{SDEP}, is mainly dependent on the supersaturation with respect to ice. Based on the depositional growth of snow crystals given by Byers (1965) with a modified ventilation effect, the equation for P_{SDEP} is given as

$$P_{SDEP} \text{ (or } P_{SSUB}) = \frac{2\pi(S_i - 1)}{\rho(A'' + B'')} n_{0S} \left[0.78\lambda_S^{-2} + 0.31 S_c^{1/3} \Gamma\left(\frac{d+5}{2}\right) c^{1/2} \left(\frac{\rho_0}{\rho}\right)^{1/4} \nu^{-1/2} \lambda_S^{-(d+5)/2}\right],$$

where

$$A'' = \frac{L_S^2}{K_a R_w T^2}, \quad B'' = \frac{1}{\rho r_{si} \psi}, \quad (31)$$

and we have assumed that the ventilation of heat is equal to that of mass, and that the ventilation coefficient for snow takes the same form as that determined by Beard and Pruppacher (1971) for small raindrops. From (31), sublimation (a negative contribution) occurs if the air is subsaturated with respect to ice, i.e., $S_i < 1$. An indicator δ_1 as defined in (20) is applied such that P_{SDEP} and P_{SSUB} will not occur simultaneously. Deposition occurs inside a cloud only when the temperature is lower than 0°C. From (20), P_{SSUB} is a sink term for snow when $T < 0$°C and the snow is outside the cloudy region. Although these two terms P_{SDEP} and P_{SSUB} can be combined as a single term and thereby eliminate the need for δ_1, we chose to keep them separate to provide a more thorough accounting of these terms.

4) Melting

The melting of snow is treated in a fashion analogous to that used for melting of hail by Mason (1971) and Wisner *et al.* (1972). The melting rate is based on heat balance considerations with the cooling associated with the melting being balanced by the combined effects of conduction and convection of heat to the particle surface, the latent heat of condensation and evaporation of water to or from the particle surface, and the sensible heat associated with the accreted water. The rate of melting of snow to form rain can be expressed as

$$P_{SMLT} = -\frac{2\pi}{\rho L_f}(K_a T_c - L_v \psi \rho \Delta r_s) n_{0S} \left[0.78\lambda_S^{-2} + 0.31 S_c^{1/3} \Gamma\left(\frac{d+5}{2}\right) c^{1/2} \left(\frac{\rho_0}{\rho}\right)^{1/4} \nu^{-1/2} \lambda_S^{-(d+5)/2}\right] - \frac{C_w T_c}{L_f}(P_{SACW} + P_{SACR}). \quad (32)$$

In (32) we have employed the same assumptions regarding the ventilation coefficient noted for (31) and have assumed that the collected and melted water is at the air temperature T_c rather than the wet bulb temperature, which is more physically appropriate (Kinzer and Gunn, 1951). Rasmussen and Pruppacher (1982) have investigated the melting of small frozen drops experimentally and theoretically and have shown that theory underpredicts the melting

rate. They attribute the difference to the role of internal circulation in the water film. Another interesting aspect of their study was the experimental demonstration of the role of the vapor transfer term in delaying the onset of melting until several degrees above 0°C in evaporative conditions. Whether the result is heating or cooling, the thermal effect of the mass change due to the vapor transfer is significant to the melting process, whereas the mass transfer rate via the vapor phase is generally insignificant compared to the melting rate. In this study, we shall ignore the mass transfer via the vapor phase for ice particles in the temperature regime $T \geqslant T_0$.

5) THE BERGERON PROCESS

In this model, cloud water and cloud ice are permitted to coexist between 0 and −40°C. The Bergeron process simulated in Orville and Kopp (1977) is modified to a more realistic scheme developed by Hsie *et al.* (1980) and is used as a generation mechanism for snow instead of hail as originally developed.

Two terms, P_{SFW} and P_{SFI}, describe the rates at which cloud water and cloud ice, respectively, transform to snow by deposition and riming based on the growth of a 50 μm radius ice crystal. The equations for these rates may be written as

$$P_{\text{SFW}} = N_{I50}(a_1 m_{I50}^{a_2} + \pi E_{IW} \rho l_{CW} R_{I50}^2 U_{I50}), \quad (33)$$

$$P_{\text{SFI}} = l_{CI}/\Delta t_1, \quad (34)$$

where a_1 and a_2 are temperature-dependent parameters in the Bergeron process (taken from Koenig, 1971) and R_{I50}, m_{I50} and U_{I50} are the radius, mass and terminal velocity of a 50μm size ice crystal. N_{I50} is the number concentration (g^{-1}) of the 50 μm size ice crystals and E_{IW} is the collection efficiency of cloud ice for cloud water which is assumed to be 1 in this model. For more information, including a discussion of the temperature-dependent time scale Δt_1, the reader is referred to Hsie *et al.* (1980).

6) TRANSFORMATION RATES FOR SNOW

Fig. 3 shows several of the production terms for snow for certain values of snow, rain, hail, cloud ice or cloud water, and for representative environmental conditions. The abscissa represents the bulk water content of the accreting particles. The ordinate gives the transformation rates in grams per gram per second. The curve for P_{SMLT} is computed at +5°C and water saturation conditions.

Some additional points are described here. Note that in Fig. 3, P_{RACS} is greater than P_{GACS}. This can be explained by examining the total number concentration of accreting particles N_t. For precipitating particles, N_t equals n_{0R} (or n_{0G}, n_{0S} for hail and snow, respectively) divided by λ_R (or λ_G, λ_S). The calculations show that the concentration of raindrops is over 50 times greater than that for hail at the same water contents. This implies that given the same snow content, the rain particles will accrete snow particles more effectively than does hail, although the difference in fallspeeds offsets this to some degree. Fig. 3 also shows that P_{RACS} is greater than P_{SACR}, which again can be explained by the number concentration of the accreting particles, rain particles being a factor of 1.17 greater in number than snow particles, for the same mass contents.

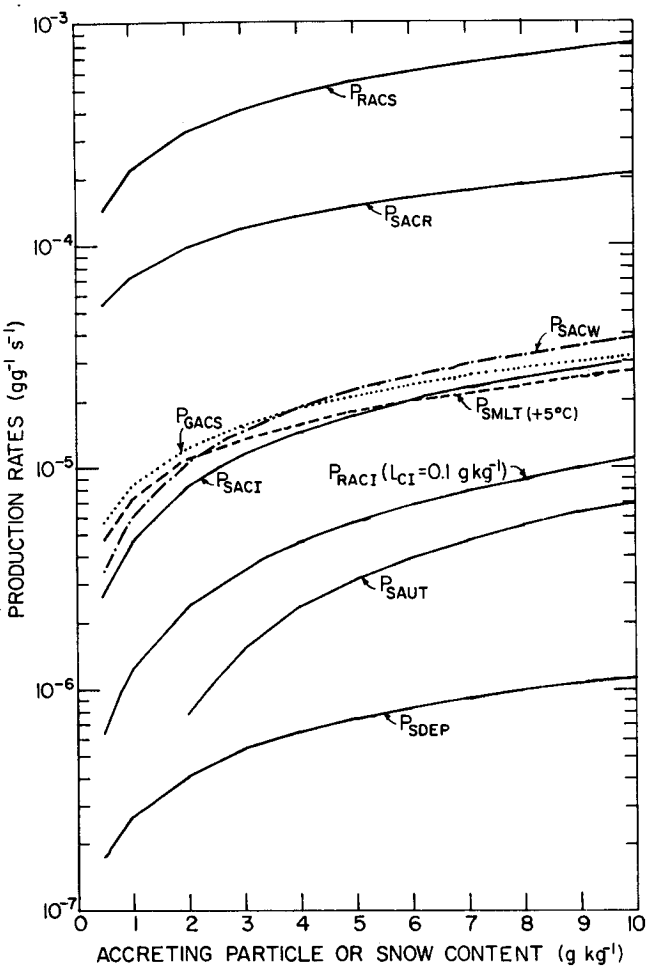

FIG. 3. Transfer rates for microphysical processes involving the snow field. The mixing ratio of the class of particle being accreted is set to be 1 g kg^{-1} unless otherwise noted.

The rate of freezing of rain via the collision-freezing mechanism between rain and cloud ice (P_{IACR}) is not depicted in Fig. 3. This rate is much larger than the other rates depicted in Fig. 3 and is a reflection of the fact that rain is rapidly frozen in the presence of small amounts of cloud ice (Cotton, 1972). Production terms, P_{SFW} and P_{SFI}, which are also not presented in the figure, are much smaller than the other terms shown. For l_{CI} fixed at 10^{-6} g g^{-1}, P_{SFW} ranges from

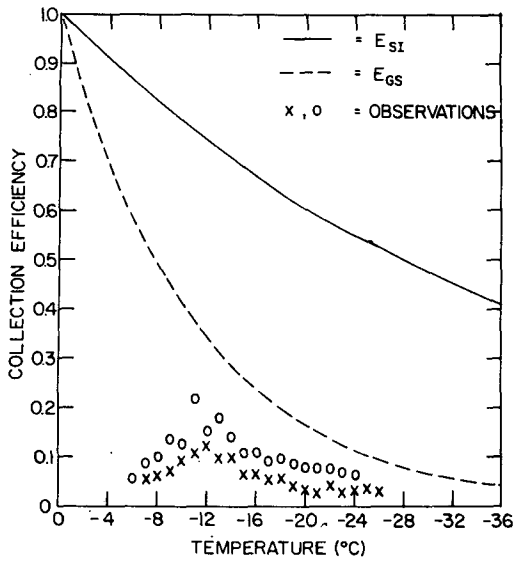

FIG. 4. Collection efficiencies assumed in the model compared with laboratory observations. The symbol × is for 127 μm spheres collecting 8–18 μm crystals. The symbol O is for 360 μm spheres collecting 8–18 μm crystals (Hosler and Hallgren, 1961).

about 4.5×10^{-11} g g^{-1} s^{-1} to 6.9×10^{-10} g g^{-1} s^{-1}, when l_{CW} is in the range of 10^{-4} to 10^{-2} g g^{-1}, P_{SFI} ranges from 8.8×10^{-10} to 3.2×10^{-9} g g^{-1} s^{-1}, with l_{CI} in the range of 5×10^{-8} to 10^{-4} g g^{-1}.

In the production rates P_{SACI} [(22)] and P_{GACS} [(29)], we used assumed collection efficiencies E_{SI} and E_{GS}, given respectively by (23) and (30). A similar temperature dependence has been assumed for the rate coefficients for P_{SAUT} [(21)] and P_{GAUT} [(37)]. Unfortunately, there have been few experimental studies of ice collecting ice and no theoretical studies due to the complexity of the problem. Fig. 4 compares the assumed collection efficiencies to the values derived from laboratory studies as reported by Hosler and Hallgren (1961). The obvious disagreement between the assumed and observed collection efficiencies is due to the fact that the observed values were obtained at ice saturation. In a related study, Hosler *et al.* (1957) note considerably higher efficiencies at ice supersaturation, the efficiency increasing with increasing temperature. In a somewhat different vein, Passarelli (1978) deduced a mean aggregation efficiency of 1.4 ± 0.6 from aircraft data. He noted efficient aggregation extended down to the −12 to −15°C range and attributed the difference between his findings and laboratory studies to the fact that nature produces more elaborate crystals and larger sizes. The assumed collection efficiencies reflect the results quoted above in a number of ways:

(i) The assumed efficiencies, especially E_{GS}, are close to the observations at low temperatures where ice saturation is more likely.

(ii) Efficiencies are highest at 0°C, consistent with the indirect evidence of efficient aggregation in this region provided by the radar "bright band."

(iii) The trend to higher than observed values in the intermediate temperature range seems justified due to the likelihood of ice supersaturation in this regime.

(iv) E_{SI} is greater than E_{GS} consistent with the relative ease with which ice crystals are collected by snow crystals as opposed to hard ice spheres as indicated by Nakaya (1954).

d. Production term for hail

Both dry and wet growth of hail are considered in this model, while only dry growth is considered in Chang (1977).

The total production term for hail can be written as:

(i) If the temperature is below 0°C ($T < T_0$):

$$P_G = P_{GAUT} + P_{GFR} + P_{GDRY} \text{ (or } P_{GWET}) + P_{SACR}(1 - \delta_2) + P_{RACS}(1 - \delta_2) + P_{RACI} \times (1 - \delta_3) + P_{IACR}(1 - \delta_3) + P_{GSUB}(1 - \delta_1). \quad (35)$$

(ii) If the temperature is above 0°C ($T \geq T_0$):

$$P_G = P_{GMLT} + P_{GACS}. \quad (36)$$

The definition of δ_1, δ_2 and δ_3 are given by (20). The two sets of coupled terms present in (35) [P_{RACI}, P_{IACR} and P_{RACS}, P_{SACR}], are given earlier by (25), (26) and (27), (28). For P_{RACI} and P_{IACR}, hail will be produced only when the mixing ratio of rain (l_R) exceeds 10^{-4} g g^{-1}. For P_{SACR} and P_{RACS}, hail production results when the mixing ratio of either rain or snow exceeds 10^{-4} g g^{-1}.

1) SNOW CRYSTAL AGGREGATION

Rimed snow crystals may collide and aggregate to form graupel or hail. The aggregation rate is assumed to follow the form used to express the aggregation of cloud ice to form snow [Eq. (21)]. The aggregation rate may be expressed as

$$P_{GAUT} = \alpha_2(l_S - l_{S0}), \quad (37)$$

where α_2 is a rate coefficient (s^{-1}), and l_{S0} is a mass threshold for snow; l_{S0} is set somewhat arbitrarily at 6×10^{-4} g g^{-1} as in Chang (1977). The rate coefficient α_2 is assumed to be temperature dependent and is given as

$$\alpha_2 = 10^{-3} \exp[0.09(T - T_0)]. \quad (38)$$

Note that the temperature dependence of the rate coefficient is the same as that used for the collection efficiency of hail for snow [(30)].

2) ACCRETION

Hail grows by accretion of other water forms in either the dry or wet growth mode, with the applied rate being the smaller of the two. The dry growth rate P_{GDRY} is the sum of the individual hail accretion terms and can be expressed as

$$P_{GDRY} = P_{GACW} + P_{GACI} + P_{GACR} + P_{GACS}, \quad (39)$$

where P_{GACS} is given by (29). The rates of hail accreting cloud water (P_{GACW}), cloud ice (P_{GACI}) and rain (P_{GACR}) are described more completely in Orville and Kopp (1977) and Wisner *et al.* (1972), and may be written as

$$P_{GACW} = \frac{\pi E_{GW} n_{0G} l_{CW} \Gamma(3.5)}{4\lambda_G^{3.5}} \left(\frac{4g\rho_G}{3C_D\rho}\right)^{1/2}, \quad (40)$$

$$P_{GACI} = \frac{\pi E_{GI} n_{0G} l_{CI} \Gamma(3.5)}{4\lambda_G^{3.5}} \left(\frac{4g\rho_G}{3C_D\rho}\right)^{1/2}, \quad (41)$$

$$P_{GACR} = \pi^2 E_{GR} n_{0G} n_{0R} |U_G - U_R| \left(\frac{\rho_W}{\rho}\right) \times \left(\frac{5}{\lambda_R^6 \lambda_G} + \frac{2}{\lambda_R^5 \lambda_G^2} + \frac{0.5}{\lambda_R^4 \lambda_G^3}\right). \quad (42)$$

In the above, E_{GR} and E_{GW} are collection efficiencies of ice for water and are assumed to be 1. E_{GI} is assumed to be 0.1 and 1 for dry and wet growth, respectively. P_{GACS} is also a source term for hail when the temperature is warmer than 0°C, allowing for the fact that melting snow could be collected and retained by melting hail.

The equation for wet growth of hail, P_{GWET}, is based on Musil (1970) modified to include the accretion of snow and subsequently integrated over all hail sizes. The rate may be written as

$$P_{GWET} = \frac{2\pi n_{0G}(\rho L_v \psi \Delta r_s - K_a T_c)}{\rho(L_f + C_w T_c)} \times \left[0.78\lambda_G^{-2} + 0.31 S_c^{1/3} \Gamma(2.75) \left(\frac{4g\rho_G}{3C_D}\right)^{1/4} \nu^{-1/2} \lambda_G^{-2.75}\right] + (P'_{GACI} + P'_{GACS}) \left(1 - \frac{C_i T_c}{L_f + C_w T_c}\right), \quad (43)$$

where L_v is the latent heat of vaporization, $\Delta r_s = r_{s0} - r$, the water vapor mixing ratio difference between the hailstone (r_{s0}) at temperature 0°C and the environment (r), ψ is the molecular diffusion coefficient of water, K_a the thermal conductivity of air, T_c the Celsius temperature, and C_w, C_i, the specific heats of water and ice, respectively. As was noted earlier in the discussion of (32), it is the thermal effect of the vapor transfer that is of primary significance and we ignore the mass transfer via the vapor phase during wet growth.

We shall now discuss implications of the wet growth process in more detail. If all of the liquid that is collected cannot be frozen, wet growth results and shedding of water drops can occur. These shed drops are assumed to be larger than cloud droplets so shedding adds to the rain content. If P_{GWET} is selected as the proper mode for hail growth, the amount of rain actually frozen or shed is given by

$$P'_{GACR} = P_{GWET} - P_{GACW} - P'_{GACI} - P'_{GACS}, \quad (44)$$

where P'_{GACI} is given by (41) with E_{GI} set equal to 1 instead of 0.1, and similarly P'_{GACS} is given by (29) with E_{GS} set equal to 1 instead of as calculated via (30). The quantity ($P_{GWET} - P'_{GACI} - P'_{GACS}$) is the wet growth due to the liquid water collected. If P_{GACW} is less than ($P_{GWET} - P'_{GACI} - P'_{GACS}$), then P'_{GACR} is positive and some of the rain is frozen to hail. If, on the other hand, P'_{GACR} is negative, some of the cloud water collected by the hail is unable to freeze and is shed as rain. By way of example, if wet growth can freeze 10 units of liquid water, of which 5 units are accreted from rain and 7 units accreted from cloud water, giving us 12 units of liquid, then 2 units of liquid are shed as rain so that only a net of 3 units of rain are frozen; we get 2 of the 5 rain units back. [In (44), P'_{GACR} is positive and some of the accreted rain is frozen.] On the other hand, if again wet growth can freeze 10 units and rain accreted by hail is 2 units and cloud water accretion is 13 units, then the rain content actually increases by 3 units. The rain content not only retains the 2 units apparently lost to accretion, but in addition gains 3 units from the shed cloud water (P'_{GACR} is negative). This shedding mechanism may cause rapid transformation of cloud to rain and occurs primarily in the 0 to −10°C region of the cloud. In addition, any collision of hail with cloud water in cloud regions warmer than 0°C results in transformation of the cloud water to rain through shedding (melting is also occurring, transforming hail to rain).

3) RAINDROP FREEZING

The equation for raindrop freezing is based on the work of Bigg (1953) and represents the formation of hail from raindrops due to immersion freezing, as explained in Wisner *et al.* (1972). It may be written as

$$P_{GFR} = 20\pi^2 B' n_{0R} \left(\frac{\rho_W}{\rho}\right) \times \{\exp[A'(T_0 - T)] - 1\}\lambda_R^{-7}, \quad (45)$$

where B' and A' are parameters in the Bigg freezing process as determined from laboratory experiments.

4) SUBLIMATION

If hail falls out of a cloudy environment, then sublimation will occur in a subsaturated region. Similar to (31), we obtain the equation

$$P_{\text{GSUB}} = \frac{2\pi(S_i - 1)}{\rho(A'' + B'')} n_{0G}\left[0.78\lambda_G^{-2} + 0.31S_c^{1/3}\Gamma(2.75) \times \left(\frac{4g\rho_G}{3C_D\rho}\right)^{1/4} \nu^{-1/2}\lambda_G^{-2.75}\right]. \quad (46)$$

The $(S_i - 1)$ in (46) is negative in the subsaturated region and thus P_{GSUB} is a sink term for hail content.

5) MELTING

The melting of hail is based on heat balance considerations as described in Mason (1971) and Wisner *et al.* (1972). The melting rate P_{GMLT} is given by

$$P_{\text{GMLT}} = -\frac{2\pi}{\rho L_f}(K_a T_c - L_v\psi\rho\Delta r_s)n_{0G} \times \left[0.78\lambda_G^{-2} + 0.31S_c^{1/3}\Gamma(2.75) \times \left(\frac{4g\rho_G}{3C_D}\right)^{1/4} \nu^{-1/2}\lambda_G^{-2.75}\right] - \frac{C_w T_c}{L_f}(P_{\text{GACW}} + P_{\text{GACR}}). \quad (47)$$

The discussion of the physics involved in this rate has already been provided in the development of the melting rate for snow, P_{SMLT} [(32)]. The findings of Rasmussen and Pruppacher (1982) noted in the discussion of (32), are especially relevant to (47). In the current formulation, the accreted cloud water is shed as rainwater and represents another source of rain from cloud water.

e. Production term for rain

Similar to the previous sections, we consider the total production rate first. The total production term for rain can be written as:

(i) If the temperature is below 0°C ($T < T_0$):

$$P_R = P_{\text{RAUT}} + P_{\text{RACW}} - P_{\text{IACR}} - P_{\text{SARC}} - P_{\text{GACR}} \text{ (or } P'_{\text{GACR}}) - P_{\text{GFR}} + P_{\text{REVP}}(1 - \delta_1). \quad (48)$$

(ii) If the temperature is above 0°C ($T \geq T_0$):

$$P_R = P_{\text{RAUT}} + P_{\text{RACW}} + P_{\text{SACW}} + P_{\text{GACW}} - P_{\text{GMLT}} - P_{\text{SMLT}} + P_{\text{REVP}}(1 - \delta_1). \quad (49)$$

The terms are described below.

1) AUTOCONVERSION

The collision and coalescence of cloud droplets to form raindrops is parameterized using a modified form of the relation suggested by Berry (1968). It may be written as

$$P_{\text{RAUT}} = \rho(l_{CW} - l_{W0})^2[1.2 \times 10^{-4} + \{1.569 \times 10^{-12}N_1/[D_0(l_{CW} - l_{W0})]\}]^{-1}, \quad (50)$$

where N_1 is the number concentration of cloud droplets and D_0 the dispersion, with l_{W0}, a threshold for autoconversion, set equal to 2×10^{-3} g g^{-1}. When the amount of cloud water exceeds l_{W0}, there is a probability of forming raindrops. The introduction of the threshold in (50) is an empirical modification to Berry's original form made to better simulate observations of first echoes. For cold-based clouds typical of the northern High Plains region, we normally turn off P_{RAUT} consistent with observations which indicate the collision-coalescence process is rarely active (Dye *et al.*, 1974). The value of N_1 and D_0 used in this study are consistent with the continental nature of the clouds but, even with the modification, do not provide adequate suppression of the process. Therefore we regard Case 3, which does not allow this process, to be more realistic, especially with regard to precipitation initiation.

2) ACCRETION

Raindrops, once formed, continue to grow by accretion of cloud water. By applying the geometric sweep-out concept and integrating over all raindrop sizes, this rate is given as

$$P_{\text{RACW}} = \frac{\pi E_{RW} n_{0R} a l_{CW}\Gamma(3 + b)}{4\lambda_R^{3+b}}\left(\frac{\rho_0}{\rho}\right)^{1/2}, \quad (51)$$

where the collection efficiency E_{RW} is assumed to be 1. This rate is the same as that used by Wisner *et al.* (1972) and Orville and Kopp (1977), except for a height correction applied to the fallspeed relationship. P_{RACW} always serves as a source term of rain content, independent of temperature regime.

In the temperature region $T < 0$°C, there are three additional accretion terms which provide negative contributions to the rain field; they are P_{IACR}, P_{SACR} and P_{GACR} (or P'_{GACR}) given respectively by (26), (28) and (42). Two other accretion processes [P_{SACW} (24) and P_{GACW} (40)] provide positive contributions to rain if the temperature is above 0°C. This is another example of shedding in the model.

3) FREEZING AND MELTING

The freezing of raindrops P_{GFR} is a source term of hail content and is a sink term for rain content

for temperatures below 0°C. The equation is given by (45).

In the temperature region $T \geq T_0$, the melting of snow and hail contribute to the rain content. These rates, P_{SMLT} and P_{GMLT}, have already been shown in (32) and (47).

4) EVAPORATION

The evaporation rate of rain is according to the concepts of diffusional growth originally developed by Byers (1965) and is described in Orville and Kopp (1977):

$$P_{REVP} = 2\pi(S-1)n_{0R}\left[0.78\lambda_R^{-2} + 0.31S_c^{1/3}\Gamma[(b+5)/2]a^{1/2}\nu^{-1/2}\left(\frac{\rho_0}{\rho}\right)^{1/4}\lambda_R^{-[(b+5)/2]}\right] \times \left(\frac{1}{\rho}\right)\left(\frac{L_v^2}{K_a R_w T^2} + \frac{1}{\rho r_s \psi}\right)^{-1}, \quad (52)$$

where R_w is the gas constant for water vapor, r_s the saturation mixing ratio of water vapor, and S the saturation ratio r/r_s (here <1). The evaporation of rain is applied only in the subsaturated air.

f. Non-precipitating fields

The non-precipitating fields, water vapor, cloud water and cloud ice, are treated as a single combined quantity in the conservation equation given by (14). The production terms involving the various types of precipitating particles and the water vapor, cloud water and cloud ice fields have been presented in previous sections. Several of these terms cancel out if total production terms P_R, P_S and P_G in (14) are expanded to the individual terms, leaving only those terms with impact on the non-precipitating fields. This results in water vapor being depleted by P_{SDEP} (31) and created by P_{SSUB} (31), P_{GSUB} (46) and P_{REVP} (52). Cloud water is depleted by P_{SACW} (24), P_{SFW} (33), P_{GACW} (40), P_{RAUT} (50) and P_{RACW} (51), while cloud ice is depleted by P_{SAUT} (21), P_{SACI} (22), P_{RACI} (25), P_{SFI} (34) and P_{GACI} (41).

Saturation is diagnosed following the treatment given by Orville and Kopp (1977). In addition, the interactions between cloud water and cloud ice which are allowed in the model have yet to be described. These are explained in greater detail in Hsie *et al.* (1980), and only a brief summary will be given here.

If the temperature is colder than −40°C, homogeneous nucleation (denoted as P_{IHOM}) will occur naturally. Saunders' (1957) equation of isobaric freezing for cloud water into cloud ice is used to calculate the temperature change associated with this process. Between 0 and −40°C, cloud water and cloud ice can coexist. The transformation between cloud water and cloud ice in this temperature regime (denoted as P_{IDW}) is based on deposition nucleation of natural ice nuclei and depositional growth of cloud ice at the expense of cloud water [Bergeron process, based on Koenig (1971)]. The number concentration of active natural ice nuclei is given by Fletcher (1962) as

$$N_n(\Delta T) = n_0 \exp(\beta \Delta T),$$

where ΔT is the supercooling and n_0 and β are parameters with values of β ranging between 0.4 and 0.8; n_0 can vary by several orders of magnitude. The typical values of $n_0 = 10^{-8}$ m^{-3} and $\beta = 0.5$ K^{-1} are used in this study. If the temperature is warmer than 0°C, the cloud ice is assumed to instantaneously melt back to cloud water (P_{IMLT}).

g. Dynamics and thermodynamics

1) DYNAMICS

Applying Newton's second law of motion in the 2DTD model yields equations of motion in the horizontal and vertical directions (Orville and Kopp, 1977). The non-hydrostatic, anelastic equations of motion include buoyancy effects due to loading of hydrometeors and turbulent mixing. All hydrometeors are assumed to fall at their mass-weighted mean terminal velocities.

Combining the two equations of motion and the continuity equation, we can derive a vorticity equation which is then used to obtain the velocity field (see Chen and Orville, 1980).

2) THERMODYNAMICS

The thermodynamics energy equation is based on Orville and Kopp (1977) with the effects of the snow field added. The equation is

$$\frac{\partial \phi'}{\partial t} = -\mathbf{V}\cdot\nabla\phi' + \nabla\cdot K_h\nabla\phi' + \frac{L_f}{C_pT_{00}}(P'_G + P'_S) + \frac{C_wT_c}{C_pT_{00}}(P_{GMLT} + P_{SMLT}) - \frac{C_w}{C_pT_{00}}[l_{CW}\mathbf{V}\cdot\nabla T + l_R(\mathbf{V} - \mathbf{k}U_R)\cdot\nabla T] - \frac{C_i}{C_pT_{00}}\delta[l_{CI}\mathbf{V}\cdot\nabla T + l_G(\mathbf{V} - \mathbf{k}U_G)\cdot\nabla T + l_S(\mathbf{V} - \mathbf{k}U_S)\cdot\nabla T, \quad (53)$$

with

$$\phi' = \frac{\theta'}{\Theta} + \frac{Lr}{C_pT_{00}} \text{ (unsaturated)}, \quad (54a)$$

$$\phi' = \frac{\theta'}{\Theta} + \frac{Lr_s}{C_pT_{00}} \text{ (saturated)}, \quad (54b)$$

and

$$P'_G = P_{GFR} + P_{GACW} + P_{GACR} + P_{GSUB} + (1 - \delta_2)P_{SACR} + (1 - \delta_3)P_{IACR} + P_{GMLT}, \quad (55)$$

$$P'_S = P_{SFW} + P_{SACW} + \delta_2 P_{SACR} + \delta_3 P_{IACR} + \delta_1 P_{SDEP} + (1 - \delta_1)P_{SSUB} + P_{SMLT}. \quad (56)$$

In (53), T_{00} is a reference temperature and ϕ' is related to entropy and equivalent potential temperature. Additionally, δ is 1.0 for $T < 0$°C and 0 otherwise, and U_R, U_G, U_S represent terminal velocities for rain, hail and snow, respectively, and $\mathbf{k}$ is the unit vector in the z-direction.

The first two terms on the right-hand side of (53) represent the advection and turbulent mixing effects. The third term shows the heating effect when freezing liquid water, or a cooling effect when melting, or part of the sublimational cooling effect when hail and snow are outside a cloudy environment. The fourth term indicates the energy needed to warm the melted hail and snow from 0°C to the ambient temperature. The last two terms represent the energy changes due to the various hydrometeors coming into thermal equilibrium with the environment as they move through a temperature gradient. For subsaturated conditions, the wet-bulb temperature is actually more appropriate for rain and melting snow and hail than the environmental temperature used here (Kinzer and Gunn, 1951).

4. Boundary and initial conditions and numerical techniques

a. Boundary conditions

Since the domain in the cloud model is limited, boundary conditions must be specified along all sides of the model domain. The treatment of boundary conditions can have a significant impact on model results, as is indicated by the considerable amount of interest and research being devoted to the problem. The boundary conditions applied in this model will now be described.

The top boundary is assumed to be rigid with all variables held constant. The vorticity, vertical velocity, rain, snow, hail, cloud water, and cloud ice are all set to zero. The stream function, entropy, and water vapor mixing ratio are maintained undisturbed at their initial values.

At the lower boundary, the vertical velocity, vorticity and streamfunction are set to zero. Evaporation and heating rates at the surface are prescribed. Heat and water vapor are allowed to diffuse into the lower boundary. The cloud is not permitted to form at the surface, but precipitation is allowed to fall through the surface level.

At the lateral boundaries, the treatment is different from an earlier treatment of lateral boundary conditions in Orville and Kopp (1977). In the old treatment, the horizontal gradients were set equal to zero at the lateral boundaries as follows:

$$X(1, K) = X(2, K) \quad \text{and} \quad X(97, K) = X(96, K)$$

so that actually

$$\frac{\partial X}{\partial x} = 0 \quad \text{at} \quad J = 1\text{½}, 96\text{½},$$

where $X(J, K)$ is a variable on the grid point (J, K), J and K vary from 1 to 97; $J = K = 1$ is the lower left-hand corner of the grid, and $J = K = 97$ is the upper right-hand corner of the grid. The new treatment is modified to keep the physics intact by using fictitious points whenever information beyond the model domain is required. In other words, we establish fictitious points, $(0, K)$ and $(98, K)$, and let

$$X(0, K) = X(2, K) \quad \text{and} \quad X(98, K) = X(96, K),$$

so that

$$\frac{\partial X}{\partial x} = 0 \quad \text{at} \quad J = 1, 97,$$

i.e., the centered horizontal derivative of all variables at a lateral boundary is assumed to be zero. The vertical velocity along the lateral boundary is zero because $\partial\psi/\partial x = 0$ there. Boundary conditions for the advection calculations are slightly different. For inflow boundaries the second derivative is also zero. That is to say

$$X(1, K) = X(2, K) \quad \text{and} \quad X(97, K) = X(96, K),$$

as well as the fictitious points described above. For outflow boundaries upstream differencing is used for advection. After the advection calculations are completed, the model prognostic equations are solved at the lateral boundary grid points.

b. Initial conditions

Radiosonde sounding data of temperature, humidity and pressure are used as input data. The horizontal wind in the direction of motion of the storm is reduced to allow the storm to remain in the domain. Dynamically, this approach is not on firm ground, and it would be better to subtract a mean wind from the actual winds and thus allow the domain to move. This approach will be incorporated in future work.

A warm moist bubble is used to initiate the convection; i.e., temperature and water vapor perturbations are prescribed in the boundary layer with maximum excesses at 3°C and 2 g kg^{-1}, respectively. The perturbations take the form of a sine curve distribution with its maximum at the central point of each modified horizontal layer, i.e.,

$$T' = 3 \sin[(J - 37)/24]/(K - 2), \quad J = 37, \ldots, 61,$$

$$Q'_v = (2 \times 10^{-3} \times \sin[(J - 37)/24]/(K - 2),$$

$$K = 3, \ldots, 6,$$

where T' is the temperature excess, Q'_v the water vapor excess, and J and K the horizontal and vertical indices, respectively.

c. *Numerical techniques*

The equations are solved over a 19.2 km × 19.2 km domain with 200 m grid interval in both X and Z directions. The advection technique used is that of Crowley (1968), which is of first-order accuracy in time, second-order in space. Following Marchuk and Leith (Leith, 1965), a two-step advection scheme is used; vertical advection is calculated first, horizontal advection second. Direct methods described in Rognlie and Kopp (1976) for a rectangular grid domain are used to solve the Poisson-type equation for the streamfunction (Swartztrauber and Sweet, 1975). The diffusion terms are calculated by substituting the second-order approximation of the Laplace term and the nonlinear values for the eddy coefficients.

5. Results

a. *General description*

The current model has been tested by running three comparative experiments using the sounding shown in Fig. 5. This is the sounding of 2100 GMT 21 July 1976, for Miles City, Montana, in the High Plains region. The sounding is unstable and moist and the cloud develops very quickly in response to the initiating perturbations. Condensation first occurs at 11 min.

Case 1 is run with all microphysical processes activated. Case 2 is identical to Case 1 except for the absence of the snow field. Case 3 is identical to Case 1 but with rain autoconversion turned off, consistent with observations for the region which show the collision-coalescence process is rarely active in the High Plains region.

Figs. 6a and 6b display portions of the results for the three cases. The figures depict an outline of the cloud and precipitation evolution. At 21 min (10 min after initial condensation), rain (plotted if $>10^{-3}$ g g^{-1}) first appears in the middle level of the cloud in Case 2 (no snow case) (Fig. 6a). The rain is formed initially by autoconversion of cloud water. For Case 1, rain has also formed by autoconversion, but is less

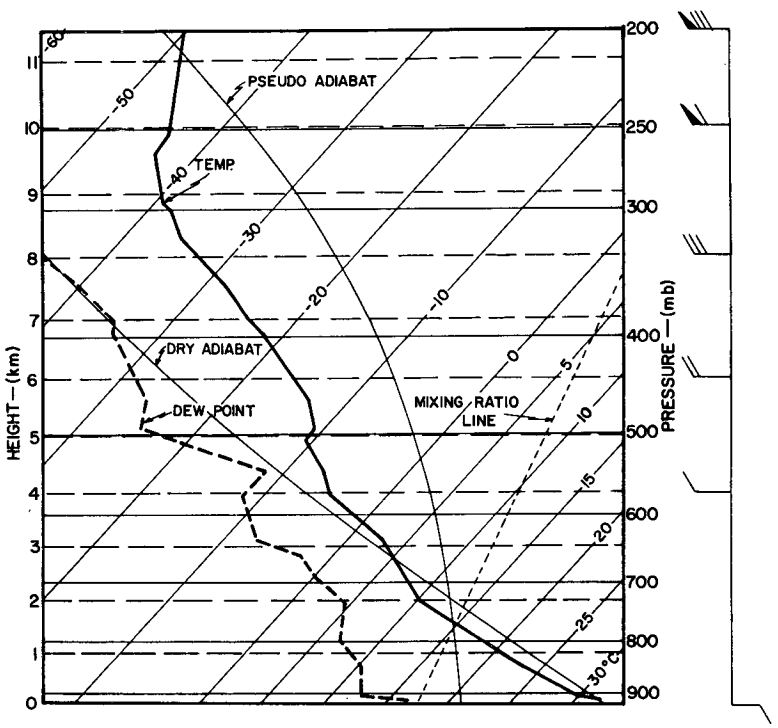

FIG. 5. The 2100 GMT atmospheric sounding for Miles City, Montana, on 21 July 1976. The horizontal winds applied in the model are also shown, with a single barb representing 1 m s^{-1} and the flag 5 m s^{-1}.

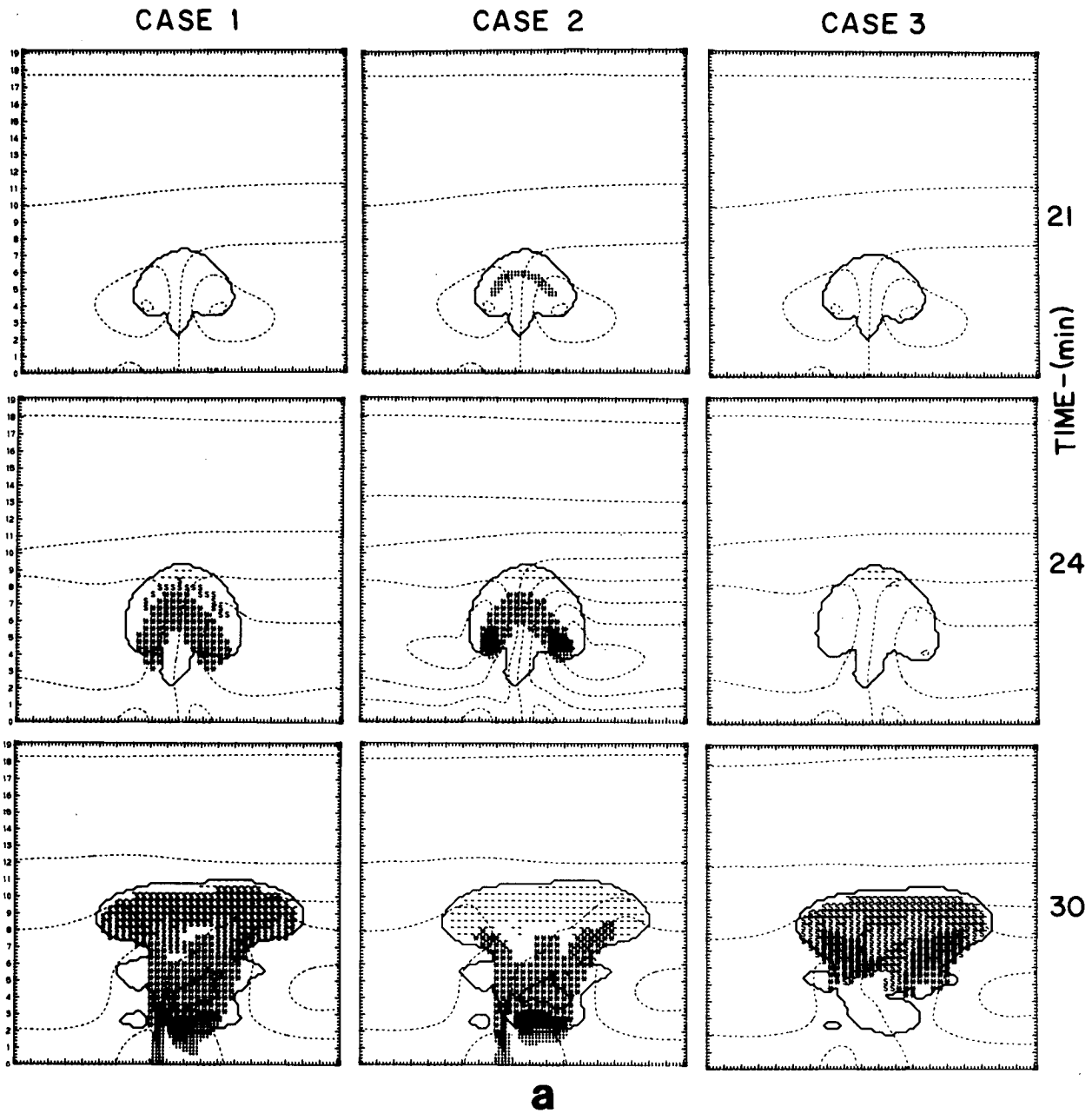

FIG. 6. Numerical simulation of cloud and precipitation for the three cases. The time evolution of Cases 1, 2 and 3 are given by the first, second and third columns, respectively. Fig. 6a shows the evolution of the three cases for the times 21, 24 and 30 min, while Fig. 6b illustrates the three cases at 36, 42 and 48 min. Cloudy areas are outlined by a solid line. The streamlines are given by dashed lines. Small solid circles and asterisks indicate rain and hail mixing ratios greater than 1 g kg^{-1}, respectively. The symbol S and the heavy dashes denote snow and cloud ice mixing ratios greater than 0.5 g kg^{-1}, respectively. The normal contour interval (10^4 kg m^{-1} s^{-1}) for the streamlines is a factor of 2 lower for times 36 and 42 min for Case 1 and 24, 36, 42 and 48 min for Case 2.

than 10^{-3} g g^{-1} because of interactions with the snow field. There is no rain yet in Case 3 (no autoconversion), and the snow field has just recently been initiated.

The freezing level is at ~3.5 km [all heights above ground level (AGL)]. Ice crystals (plotted where $l_{CI} > 5 \times 10^{-4}$ g g^{-1}) are depicted in the upper levels of the cloud in all three cases at 24 min (Fig. 6a). Snow ($>5 \times 10^{-4}$ g g^{-1}) shows up only in Case 1. At the same time, considerable amounts of hail (plotted if values $> 10^{-3}$ g g^{-1}) are indicated in Cases 1 and 2, mainly between 4 and 8 km, while rain is shown in Case 2 on both sides of the cloud between 3.5 and 5.5 km elevation. Hail has fallen to lower levels in

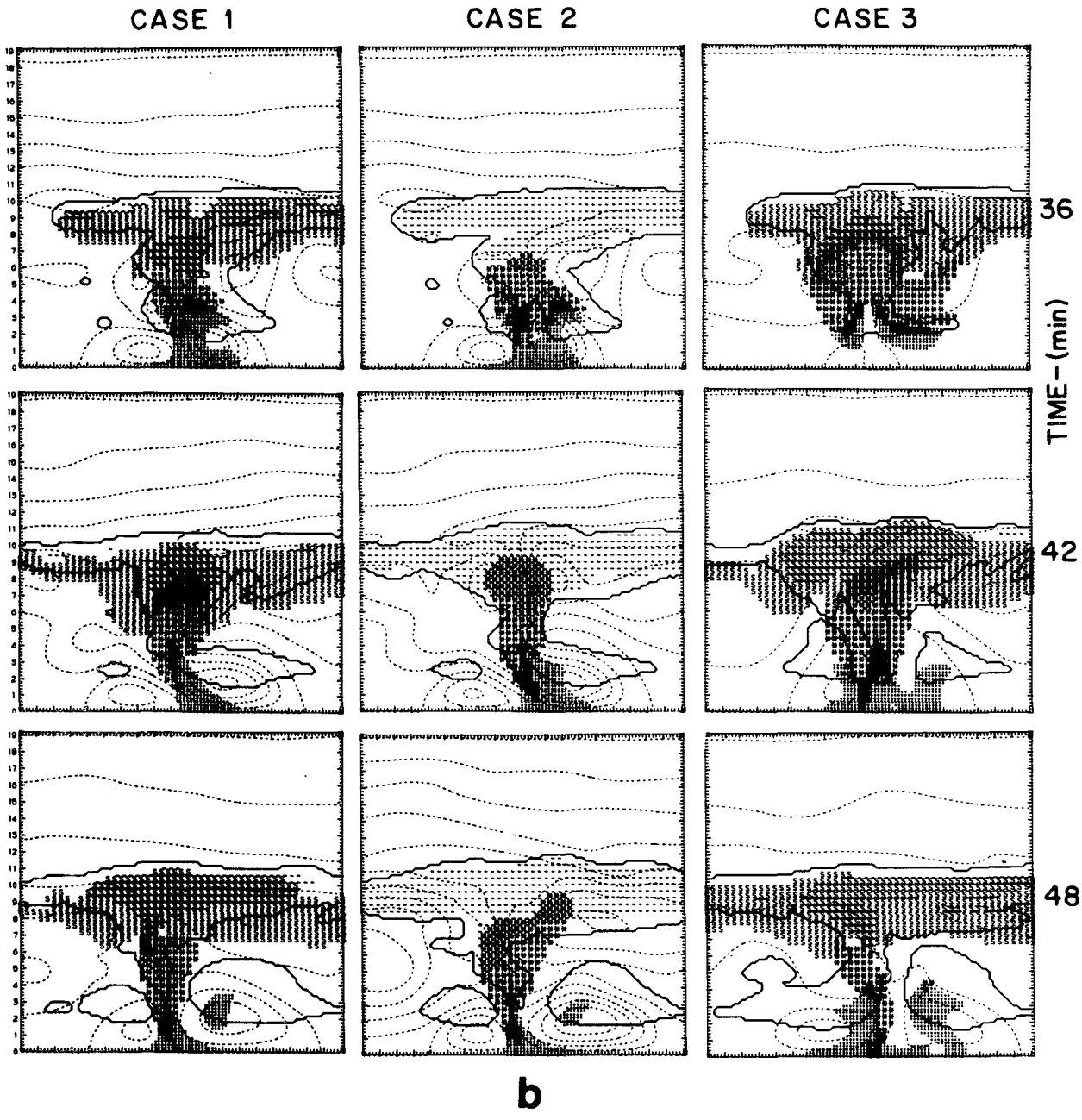

FIG. 6. (*Continued*)

Case 1 than in Case 2. The hail and snow interactions with the rain field in Case 1 have kept the rain content less than the threshold amount for plotting. None of the precipitating classes have exceeded the plotting thresholds in Case 3 at 24 min. The fields of precipitating particles (rain, snow and hail) are cap-shaped in the cloud, due to the stronger updraft in the middle of the cloud.

At 30 min (Fig. 6a), the cloud has developed to about 11 km and an anvil is forming in all cases. The cloud base is at 2 km. Considerable amounts of rain and some hail are reaching the surface at this time in Cases 1 and 2. Precipitation is appearing in the upper levels of Case 3 (no autoconversion) with the maximum of hail showing up on the sides of the main updraft. For Case 3, the primary generation mechanism for the hail up to this time is aggregation of snow (P_{GAUT}). The snow, in turn, has grown mainly by accretion of cloud water.

At 36 min (Fig. 6b), much of the cloud in Cases 1 and 3 contains some snow with virga underneath the anvil. The cloud in Cases 1 and 2 is in the later

portion of the mature stage. Surface rain and gust front formation have occurred in these cases. The precipitation fields in all cases show hail in the upper levels melting to rain in the lower levels (Fig. 6b). A very large area (volume) of hail exists in Case 3. Note that the snow is melted or evaporated before reaching the ground and is, for the most part, limited to the higher levels (above 6 km).

At 42 min (Fig. 6b), Cases 1 and 2, with active rain processes, are much more alike than Cases 1 and 3, both of which have active snow processes. Hail is being regenerated in Cases 1 and 2 due to an invigoration of the updraft. This renewed hail generation occurs mainly in the region of the cloud between 4 and 5 km AGL due to the contact freezing of rain being recycled by the invigorated updraft during the time period between 36 and 42 min. The outflow from the precipitation-induced downdraft is the primary cause of the updraft surge and hail increase. Cloud ice covers a large region in Case 2 with a maximum value of 3.6×10^{-3} g g^{-1}. Maximum values of cloud ice in Cases 1 and 3 are near 10^{-3} g g^{-1}. The presence of a snow field in Cases 1 and 3 and the lack of snow in Case 2 causes this difference. Rain has reached the surface in Case 3.

At 48 min (Fig. 6b), secondary cloud formation is evident in all three cases, the more vigorous cell on the right (lower upwind) side. The most vigorous growth of secondary cells is in Case 3.

The earlier formation and fallout of precipitation in Cases 1 and 2 compared to that in Case 3 have profound dynamic effects on the later stages of the simulations. Although not clearly evident in Fig. 6, the precipitation-induced downdraft in Case 3, while occurring later than in Cases 1 and 2, is more intense. The cascade of precipitation is also more intense and occurs over a shorter time span in Case 3. As is pointed out in Orville and Chen (1982), the timing of precipitation fallout has a strong modulating effect on storm intensity. Similar to their results, the earlier formation and fallout of precipitation in Cases 1 and 2 actually weaken subsequent storm development (the generation of daughter clouds or cells). This would be even more evident in the current results had the integrations been continued beyond 48 min.

b. Total production of rain, hail and snow

The net production of rain, hail and snow, integrated over the entire domain and accumulated to the time indicated, are shown in Figs. 7a–c for the three cases. The time evolution of the domain totals of cloud water, cloud ice, rain, snow and hail for the three cases are shown in Fig. 8. [The unit kT in Figs. 7, 8, 10, 11 and 12 is equal to 10^9 g.] Figs. 7b and 8 in conjunction with the cloud outlines in Figs. 6a and 6b show the two cells or surges in growth of the hail content for Cases 1 and 2. The two maxima occur

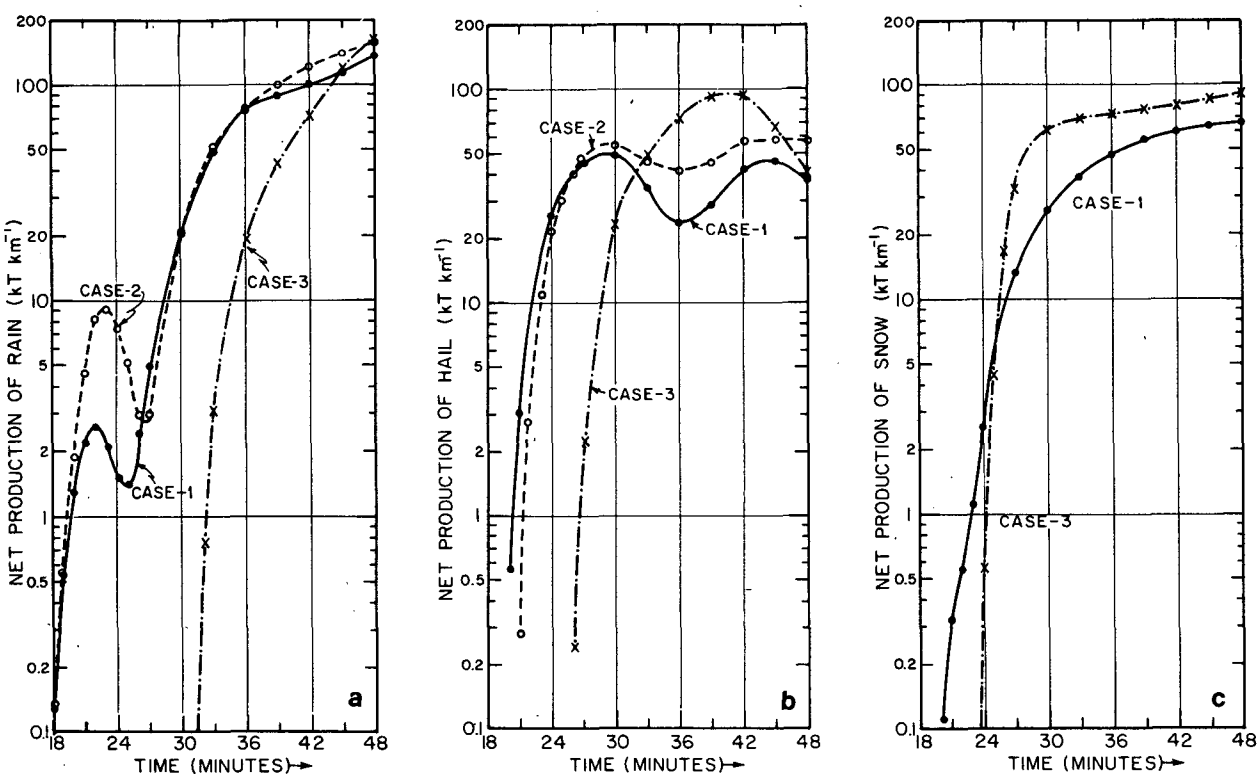

FIG. 7. The accumulated net production of (a) rain, (b) hail and (c) snow versus time for the three cases. The units of production are kT km^{-1} (10^9 g km^{-1}).

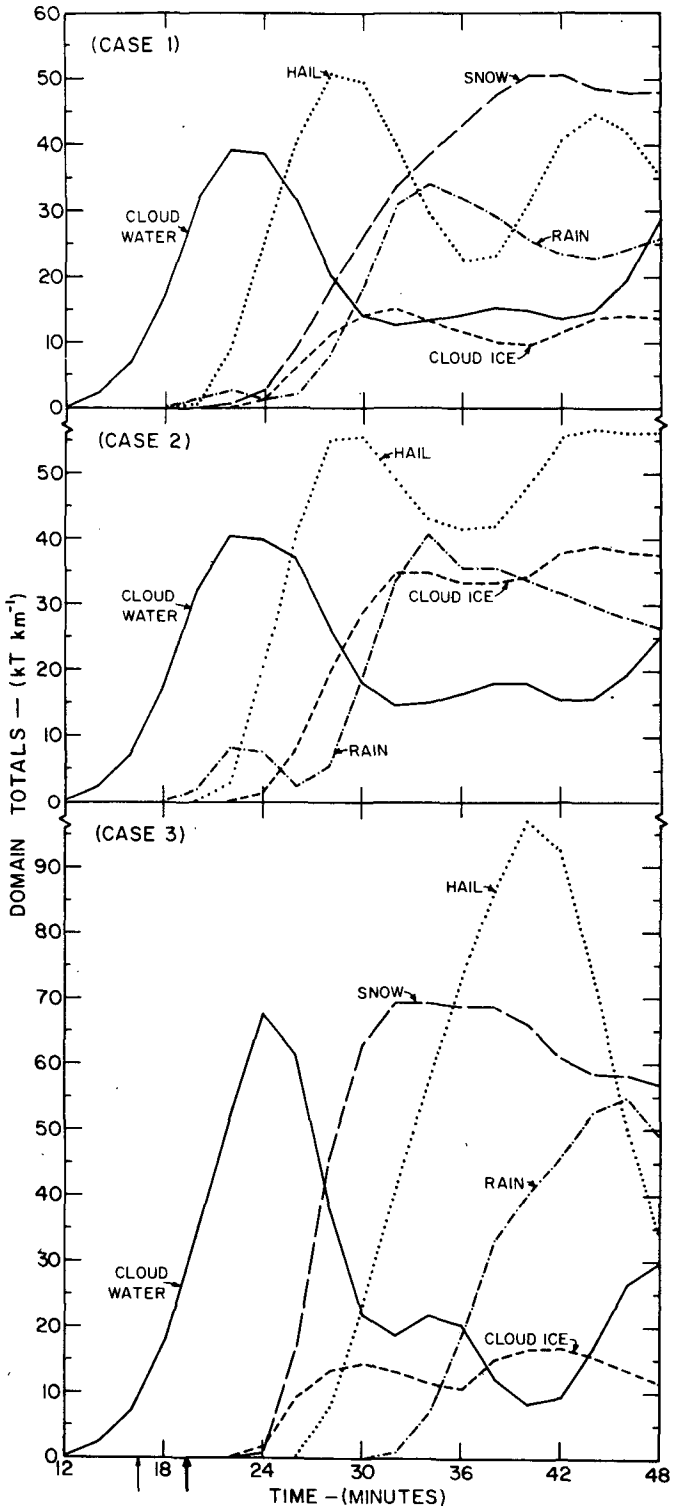

FIG. 8. The domain totals of cloud water, cloud ice, rain, snow and hail versus time for the three cases. The units are kT km^{-1}. The thin and bold arrows along the abscissa mark the times the cloud top passes −10 and −20°C, respectively, which is the same in all three cases.

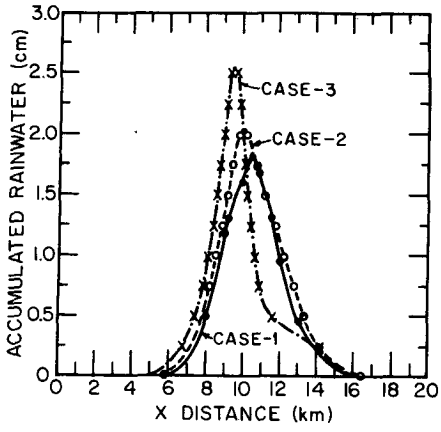

FIG. 9. The horizontal distribution of accumulated rainfall at the surface at 48 min of simulated time for the three cases.

at 29 min and 44 min in Fig. 7b and 30 min (3 km height) and 42 min (9.2 km height) in Fig. 6. The decrease in net hail production around 33 to 36 min for Cases 1 and 2 is caused by the melt of hail as it falls below the 0°C level. The fallout of precipitation at this time leads to a stimulation of the lower right portion of the cloud in Cases 1 and 2, which is responsible for the second surge in hail growth indicated in Figs. 7b and 8.

A single hail growth peak shows up in Case 3 at about 40 min (9.2 km height). Examination of Figs. 7 and 8 indicates Case 3 has rain forming nearly 12 min later than in Cases 1 and 2. However, hail formation is delayed only about 6 min. Melting of hail is the primary source of rain in all three cases, and for Case 3 it is also the initiating mechanism for rain. Rain in Cases 1 and 2 is initially produced by autoconversion. It is the freezing of this earlier rain which initiates the hail field in Cases 1 and 2 (slightly earlier in Case 1 because of rain-snow interactions). Hail in Case 3 is initiated by the aggregation of snow which occurs 6 min later than the freezing of rain in Cases 1 and 2.

The time period from 18 to 24 min in Cases 1 and 2 (Fig. 7a) indicates that the initial production of rain is followed by a temporary loss before the major rain production stage is reached. This behavior is due to the initial formation of rain in the lower level of the clouds, while the advection of rain to higher, colder levels where accretion by hail (in Case 2) or by hail and snow (in Case 1) depletes the rain. The decrease in rain ceases when hail begins to melt and becomes a dominant source of rain after 25 min.

Examination of Figs. 7 and 8 reveals that the presence of snow serves to deplete the rain field and to keep its formation rate slower in Case 1 than in Case 2 (no snow case). The snow initiates the hail field about 1 min sooner in Case 1, which results in earlier depletion of the rain in Case 1 and a reduction in the total amount of rain produced in the first surge compared to Case 2. The snow accelerates the formation of hail in Case 1, which accounts for the slightly earlier fallout of hail and associated melting to form appreciable amounts of rain. Consequently, hail is a sink for rain at first (as is snow), but a source later as it melts below the 0°C level.

Case 3 is much more inefficient in the production of precipitation in the early stages (18–30 min) as is clearly shown by the much larger amounts of cloud water (Fig. 8). Although hail production is considerably delayed in this case, the hail, once formed, is produced in much larger quantities, being present in abundant amounts throughout a greater portion of the cloud. Rain production is delayed even more, but follows the same trend as the hail in this case.

Fig. 9 shows the accumulated rain at the surface at 48 min from all three cases. Table 2 provides additional information on the results of the cases at 48 min. Some precipitation still remains to accumulate from the main cells, but these results indicate the trend of the differences. Returning to Fig. 8, we note that Cases 2 and 3 have more rain and hail (efficient precipitating forms) suspended aloft at 48 min than does Case 1. If the simulations had been continued beyond 48 min, it appears that Case 1 would remain the least efficient of the three cases. It is unclear whether Case 2 or 3 would end up producing the greatest surface accumulations since, at 48 min, Case 2 has the most hail aloft, whereas Case 3 has more rain. The no-snow case (Case 2) produces the greatest surface accumulation, presumably due to the fact that the snow process of Cases 1 and 3 depletes some of the cloud water, the snow falling out as virga evaporating before reaching the ground. Compared to the other cases, Case 2 has much larger quantities of cloud ice, which in a sense indicates less efficiency. The amount of cloud ice in Case 2, however, is less than the combined amounts of snow and cloud ice (both inefficient) in Cases 1 and 3. Case 3 produces an intermediate value of rainout but the greatest surface accumulation of hail [6.4 kT km^{-1} vs. 2.0 for Case 1, and 2.5 kT km^{-1} for Case 2]. This is due to the delay in precipitation formation which causes much of the hail to form in the upper, colder parts of the cloud; the hail thus formed must fall through

TABLE 2. Surface accumulations, total water vapor flux into storm, and precipitation efficiency at 48 min. The units for the precipitation amounts and water vapor are kT km^{-1} and 10^9 g km^{-1}.

Case	Rain at surface	Hail at surface	Total precip-itation at surface	Water vapor flux into cloud	Precip-itation efficiency (%)
Case 1	67.66	2.06	69.71	658.46	10.6
Case 2	80.45	2.49	82.93	671.82	12.3
Case 3	72.29	6.42	78.71	650.44	12.1

a greater depth of cloud leading to enhanced growth. The precipitation-induced downdraft is also more intense in Case 3 allowing less time for melting during the fall to earth. This aspect also causes the surface accumulations to be more localized, as witnessed by the more pronounced peak for Case 3 in Fig. 9.

c. *Production terms—sources and sinks*

1) HAIL

The next few figures detail the various sources and sinks involved in the production of hail, rain and snow. The various quantities plotted represent the total domain contributions of the individual processes accumulated to the time indicated. They are not rates. Figs. 10a–c show the various gain and loss terms for the production of hail. The accretional growth of hail is the biggest source term in all three cases (of order 100 kT km^{-1}). Since accretion involves all condensate, it is a summation of several terms, and can represent either dry or wet growth of hail. In general, wet growth accounts for 10% or less of the accretional growth.

The collision-freezing mechanism involving cloud ice and rain (P_{IACR}) to form hail is significant—of order 10 kT km^{-1} in all three cases. The probabilistic freezing of rain is less important in all the cases reaching a maximum value of 4 kT km^{-1} in Case 2. This term does not even show up in Case 3 (Fig. 10c).

The rain and snow interaction terms (P_{RACS}, P_{SACR}) are larger in Case 1 (7 kT km^{-1}) than in Case 3 (4 kT km^{-1}) because of the earlier appearance of snow and rain in Case 1 and the fact that rain must be initiated by melting or shedding involving precipitating ice forms (snow and hail) in Case 3.

The Bergeron process (P_{SFW}) is important in producing hail in Case 2 (of order 50 kT km^{-1}) but produces only snow in the other cases. The quantity denoted P_{GAUT} in Case 2 is the result of aggregation of cloud ice to form hail, while for Cases 1 and 3, P_{GAUT} is the result of the aggregation of snow to form hail.

The primary loss of hail is melt to rain (100 kT km^{-1}). Evaporation of hail accounts for 1 kT km^{-1} or less. The melting term shows up at 24, 26 and 32 min in Cases 1, 2 and 3, respectively, indicative of the timing of precipitation formation in the cases.

2) RAIN

The sources and sinks for rain are shown in Figs. 11a–c. The primary sources for rain are hail melt (of order 100 kT km^{-1}) and rain accretion of cloud water (ranging from 25 to 45 kT km^{-1} in the three cases).

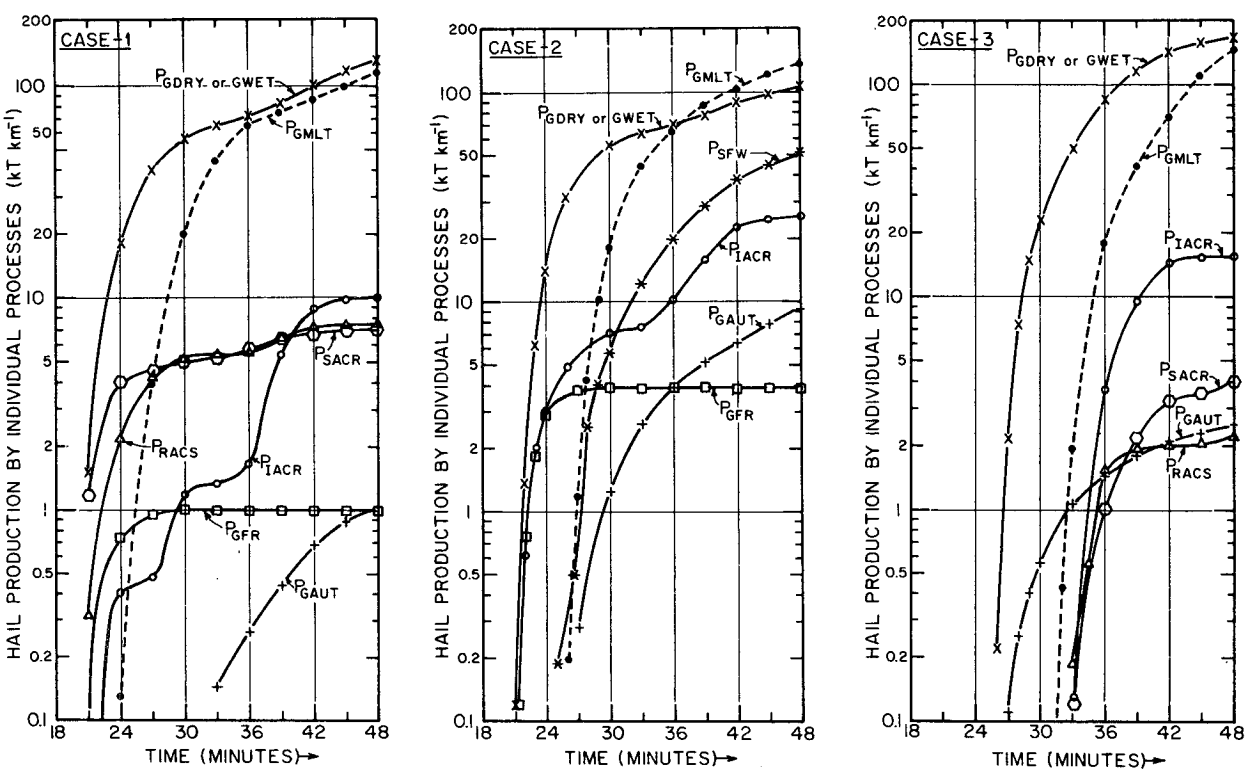

FIG. 10. The accumulated production due to individual processes contributing to a gain (solid lines) or a loss (dashed lines) of the hail field versus time for Case 1(a), Case 2(b) and Case 3(c). The units of production are kT km^{-1}. The various curves, which are labeled according to the corresponding production rates (Fig. 1 and Table 1), are the result of the various rates being integrated over the total model domain and accumulated to the time indicated.

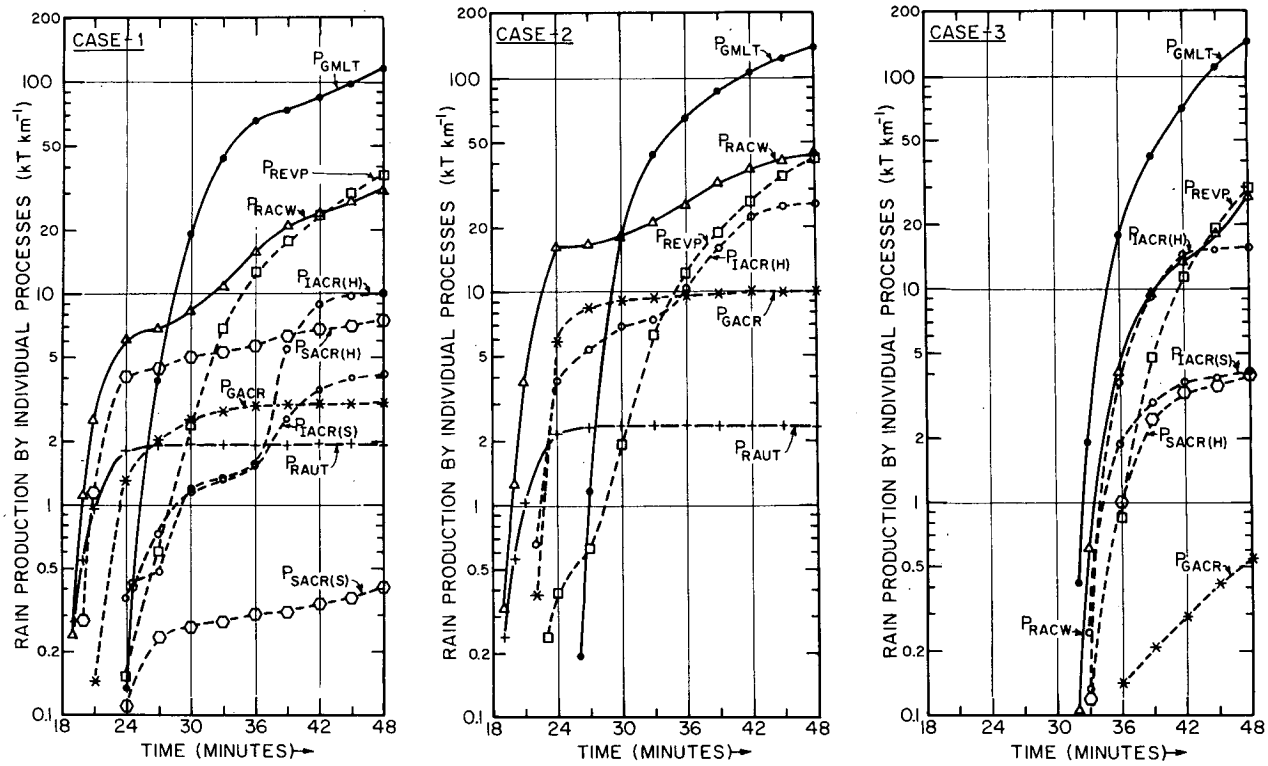

FIG. 11. As Fig. 10 except for the rain field.

Autoconversion of cloud water to form rain is small (but of crucial importance) in Cases 1 and 2 (of order 2 kT km^{-1}). Its absence in Case 3 is responsible for the later development of precipitation. Rain is delayed until hail melt begins at about 32 min in Case 3, and appears at about 18 min in the other two cases.

In Cases 1 and 2, rain initially forms in updrafts (via the P_{RAUT} and P_{RACW} terms) and then is depleted by various ice terms in the colder part of the cloud. Most of the rain that eventually falls out of the cloud is formed by melting hail for all cases.

There are several terms which contribute to the loss of rain. Evaporation is the primary sink of rain, ranging from 30 to 40 kT km^{-1} in the three cases. The next most important sink is that resulting from the accretion of rain by cloud ice (P_{IACR}, of order 20 kT km^{-1}).

Snow accreting rain to form hail results in production on the order of 10 kT km^{-1} in Cases 1 and 3.

The process of cloud ice accreting rain results in the formation of snow if the rain mixing ratio is less than 10^{-3} g g^{-1}. This process results in a total contribution of about 4 kT km^{-1} in Cases 1 and 3.

3) SNOW

Snow is produced in Cases 1 and 3 only (Figs. 12a and 12b). The primary sources of snow result from snow accreting cloud water (of order 45 and 85 kT km^{-1}) and cloud ice (of order 35 and 50 kT km^{-1}) and the Bergeron process (P_{SFW}) (of order 30 and 40 kT km^{-1} in Cases 1 and 3, respectively). The Bergeron process is the principal initiating mechanism for snow. More snow is produced in Case 3 because of the late formation of rain occurring mainly at low levels (from melting of hail) in Case 3. This allows little time for the rain to interact with the snow field and transform the snow into hail.

The aggregation of cloud ice to form snow provides a small contribution (of order 1 kT km^{-1}). Deposition contributes 4–5 kT km^{-1} to the production of snow.

The primary loss term for snow is due to the accretion of snow by hail (45 and 95 kT km^{-1} in Cases 1 and 3, respectively). Rain accretes snow to form hail more effectively in Case 1 (7 vs. 2 kT km^{-1}). Sublimation of snow accounts for ~7 kT km^{-1} loss in both cases. Aggregation of snow to form hail is very small (of order 1 kT km^{-1}) in both of these cases, but it is critically important in Case 3, being the sole initiating mechanism for the hail.

6. Conclusions and discussion

The addition of a snow field to the two-dimensional, time-dependent cloud model significantly modifies the microphysical processes compared to the model without the snow field and gives the model a

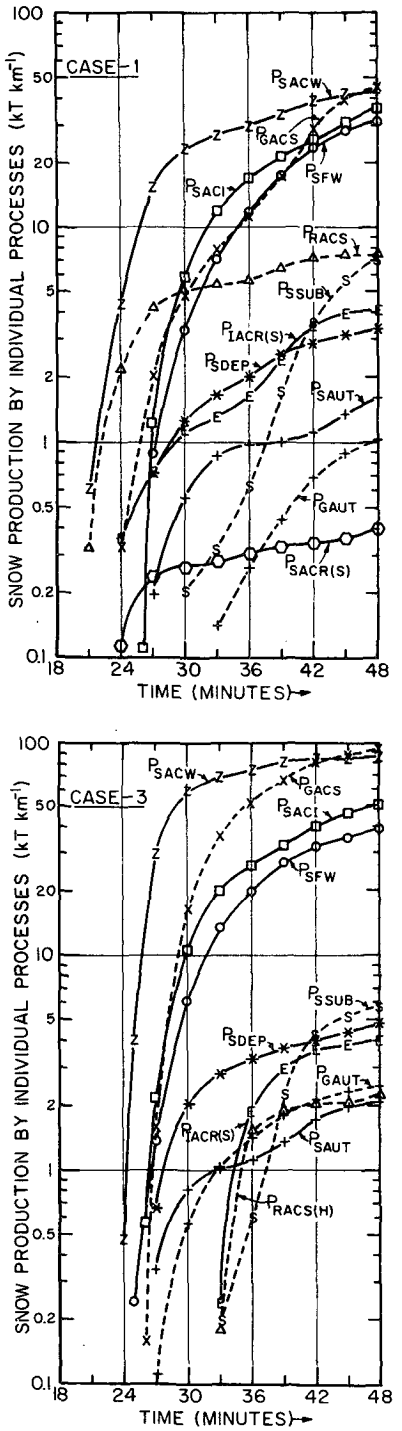

FIG. 12. As Fig. 10 except for the snow field. Figs. 12a and 12b illustrate the results for Cases 1 and 3; Case 2 results are not shown since it is a no-snow case.

greater degree of realism. Some important features are captured:

1) The transformation of cloud ice to snow and then to hail simulated in the current model is more realistic than older models where the transformation is from cloud ice to hail. The Bergeron process plays an important role in the transformation of cloud ice to snow. Additional hail is then formed by aggregation of snow particles.

2) The formation of virga from cloud anvils is now modeled.

3) The presence of the snow field serves to reduce the amount of rain forming early in the life history of the cloud.

4) The snow field significantly reduces the amount of cloud ice.

5) The delay in rain formation in Case 3 results in more hail formation but little change in total precipitation. The delay in precipitation formation has a profound effect on the dynamic evolution in the later stages.

Physical insight into the precipitation process comes from study of the production term curves and their interpretation. Suggestions as to comparisons with real data are evident but unfortunately little data are available for extensive comparison at this time. Data such as those obtained by penetrating aircraft will be particularly pertinent.

A few points highlighted by the production term figures are: (i) the major growth of hail by accretion with 10% of this by wet growth; (ii) the significance of the cloud ice and rain interactions (also as shown by Cotton (1972) in a more detailed microphysical model) to the production of snow or hail; (iii) the primary loss of hail due to melting, which is the primary source of rain even when coalescence (autoconversion) is active; (iv) the primary loss of rain due to evaporation; and (v) the importance of snow formation and growth via the Bergeron process and the accretion of cloud water and cloud ice, etc.

Several improvements and tests can be mentioned. Several microphysical assumptions need to be tested in seeding simulations and in different types of clouds. For example, a warm-based cloud will be a good case for testing. The most questionable assumptions which require additional investigation are perhaps the threshold amounts applied in the various autoconversion formulations and those used to determine the resulting hydrometeor form produced by interactions of rain and cloud ice and rain and snow.

Snow crystals are very complex. Their habits are strongly dependent on the temperature and supersaturation. In this model, only the graupel-like snow of hexagonal type is simulated. This is not sufficient to describe all kinds of snow crystals which exist in natural clouds. To improve upon it, increasing the categories of snow to approach the complex types of snow crystals or testing different types with this one category model should be done.

For the concentration of active natural ice nuclei, an exponential form suggested by Fletcher (1962) is used in the model. A more realistic representation

may be used to present some observational results by Vali (1971). These observational results indicate that low concentrations of ice nuclei active at temperatures as warm as −6°C are common, while Fletcher's curve represents the average spectrum of ice nuclei in the region −10°C to −30°C.

The most useful modification would be to add equations that predict the number concentration of the ice particles (Koenig and Murray, 1976). Cloud seeding experiments affect the number of crystals more so than the bulk mass of the ice content; therefore, seeding simulations should be more realistic with a model which predicts ice crystal number concentrations.

One of our main purposes in simulating ice processes in clouds is to use cloud models to simulate cloud seeding experiments. Hsie *et al.* (1980) have demonstrated such a use in simulating silver iodide cloud seeding experiments. Recent work with the current model involves the simulation of dry ice seeding of small convective clouds in the eastern Montana region and comparison with real data as part of the HIPLEX project. Hopefully, the model will provide physical insight for the project and the project, in turn, should provide insight into the weaknesses of the model.

Acknowledgments. We gratefully acknowledge the valuable contributions provided by Dr. Philip Chen and Chen-Hung Chang in the early stages of this work. Thanks are extended to Mr. Melvin J. Flannagan for his skillful drafting of the figures, and Mrs. Joie L. Robinson for expeditiously typing the manuscript. We also thank the reviewers for their valuable critiques which have helped improve the paper.

This research was sponsored by the Bureau of Reclamation, U.S. Department of the Interior, under Contract 8-07-83-V0009. Acknowledgment is made to the National Center for Atmospheric Research, which is sponsored by the National Science Foundation, for computer time used.

REFERENCES

Auer, A. H., 1972: Distribution of graupel and hail with size. *Mon. Wea. Rev.*, **100,** 325–328.

Beard, K. V., and H. R. Pruppacher, 1971: A wind tunnel investigation of the rate of evaporation of small water drops falling at terminal velocity in the air. *J. Atmos. Sci.*, **28,** 1455–1464.

Bergeron, T., 1935: On the physics of cloud and precipitation. *Proc. 5th Assembly IUGG,* Lisbon, 156–178.

Berry, E. X., 1968: Modification of the warm rain process. *Preprints 1st Nat. Conf. Weather Modification,* Albany, Amer. Meteor. Soc., 81–88.

Bigg, E. K., 1953: The supercooling of water. *Proc. Phys. Soc. London,* **B66,** 688–694.

Braham, R. R., Jr., 1964: What is the role of ice in summer rain-showers? *J. Atmos. Sci.*, **21,** 640–645.

Byers, H. R., 1965: *Elements of Cloud Physics.* The University of Chicago Press, 191 pp.

——, and R. R. Braham, Jr., 1949: *The Thunderstorm.* Govt. Printing Office, Washington, DC, 287 pp.

Chang, C. H., 1977: Ice generation in clouds. M.S. thesis, Dept. Meteor., South Dakota School of Mines and Technology, Rapid City, 129 pp.

Chen, C. H., and H. D. Orville, 1980: Effects of mesoscale convergence on cloud convection. *J. Appl. Meteor.*, **19,** 256–174.

Cotton, W. R., 1972: Numerical simulation of precipitation development in supercooled cumuli—Part II. *Mon. Wea. Rev.*, **100,** 764–784.

Crowley, W. P., 1968: Numerical advection experiments. *Mon. Wea. Rev.*, **96,** 1–11.

Danielsen, E. F., R. Bleck and D. A. Morris, 1972: Hail growth by stochastic collection in a cumulus model. *J. Atmos. Sci.*, **29,** 135–155.

Douglas, R. H., 1960: Size distributions, ice contents and radar reflectivities of hail in Alberta. *Nubila,* **3,** 5–11.

Dye, J. E., C. A. Knight, V. Toutenhoofd and T. W. Cannon, 1974: The mechanism of precipitation formation in northeastern Colorado cumulus, III. Coordinated microphysical and radar observations and summary. *J. Atmos. Sci.*, **8,** 2152–2159.

Federer, B., and A. Waldvogel, 1975: Hail and raindrop size distributions from a Swiss multicell storm. *J. Appl. Meteor.*, **14,** 91–97.

Findeisen, W., 1939: The evaporation of cloud and raindrops. *Meteor. Z.*, **56,** 453–460.

Fletcher, N. H., 1962: *The Physics of Rain Clouds.* Cambridge University Press, 390 pp.

Foote, G. B., and P. S. du Toit, 1969: Terminal velocity of raindrops aloft. *J. Appl. Meteor.*, **8,** 249–253.

Gagin, A., 1971: Studies of the factors governing the colloidal stability of continental cumulus cloud. *Preprints Int. Conf. Weather Modification,* Canberra, Amer. Meteor. Soc., 5–11.

Gunn, K. L. S., and J. S. Marshall, 1958: The distribution with size of aggregate snowflakes. *J. Meteor.*, **15,** 452–461.

Gunn, R., and G. D. Kinzer, 1949: The terminal velocity of fall for water drops in stagnant air. *J. Meteor.*, **6,** 243–248.

Hallett, J., R. I. Sax, D. Lamb and A. S. R. Murty, 1978: Aircraft measurements of ice in Florida cumuli. *Quart. J. Roy. Meteor. Soc.*, **104,** 631–651.

Hobbs, P. V., 1965: The aggregation of ice particles in clouds and fogs at low temperatures. *J. Atmos. Sci.*, **22,** 296–300.

——, 1974: *Ice Physics.* Oxford University Press, 837 pp.

——, 1975: The nature of winter clouds and precipitation in the Cascade Mountains and their modification by artificial seeding. Part I: Natural conditions. *J. Appl. Meteor.*, **14,** 783–804.

Hosler, C. L., and R. E. Hallgren, 1961: Ice crystal aggregation. *Nubila,* **4,** No. 1, 13–19.

——, D. C. Jensen and L. Goldshlak, 1957: On the aggregation of ice crystals to form snow. *J. Meteor.*, **14,** 415–420.

Hsie, E. Y., R. D. Farley and H. D. Orville, 1980: Numerical simulation of ice-phase convective cloud seeding. *J. Appl. Meteor.*, **19,** 950–977.

Kessler, E., 1969: *On the Distribution and Continuity of Water Substance in Atmospheric Circulations. Meteor. Monogr.*, No. 32, Amer. Meteor. Soc., 84 pp.

Kinzer, G. D., and R. Gunn, 1951: The evaporation, temperature, and thermal relaxation-time of freely falling waterdrops. *J. Meteor.*, **8,** 71–83.

Knight, C. A., and N. C. Knight, 1979: Results of a randomized hail suppression experiment in northeast Colorado: Part V. Hailstone embryo types. *J. Appl. Meteor.*, **18,** 1583–1588.

Kobayashi, T., 1957: Experimental researches on the snow crystal habit and growth by means of a diffusion cloud chamber. *J. Meteor. Soc. Japan,* 75th Anniversary Volume, 38–47.

Koenig, L. R., 1963: The glaciating behavior of small cumulonimbus clouds. *J. Atmos. Sci.*, **20,** 29–47.

——, 1971: Numerical modeling of ice deposition. *J. Atmos. Sci.*, **28,** 226–237.

——, and F. W. Murray, 1976: Ice-bearing cumulus cloud evolution: Numerical simulation and general comparison against observations. *J. Appl. Meteor.*, **15,** 747–762.

Kuettner, J., 1950: The electrical and meteorological conditions inside thunder clouds. *J. Meteor.*, **7**, 322–332.

Leith, C. E., 1965: Numerical simulation of the earth's atmosphere. *Methods in Computation Physics*, Vol. 4, *Applications in Hydrodynamics*, Academic Press.

List, R., 1960: Growth and structure of graupel and hailstones. *Geophys. Monogr.*, No. 5, Amer. Geophys. Union, 317–324.

Liu, J. Y., and H. D. Orville, 1969: Numerical modeling of precipitation and cloud shadow effects on mountain-induced cumuli. *J. Atmos. Sci.*, **26**, 1283–1298.

Locatelli, J. D., and P. V. Hobbs, 1974: Fall speeds and masses of solid precipitation particles. *J. Geophys. Res.*, **79**, 2185–2197.

Macklin, W. C., 1962: The density and structure of ice formed by accretion. *Quart. J. Roy. Meteor. Soc.*, **88**, 30–50.

Magono, C., and C. W. Lee, 1966: Meteorological classification of natural snow crystals. *J. Fac. Sci. Hokkaido Univ.*, Ser. VII, **2**, 321–335.

Marshall, J. S., and W. McK. Palmer, 1948: The distribution of raindrops with size. *J. Meteor.*, **5**, 165–166.

Mason, B. J., 1971: *The Physics of Clouds*, 2nd ed. Oxford University Press, 671 pp.

Mossop, S. C., 1978: Some factors governing ice particle multiplication in cumulus clouds. *J. Atmos. Sci.*, **10**, 2033–2037.

Musil, D. J., 1970: Computer modeling of hailstone growth in feeder clouds. *J. Atmos. Sci.*, **27**, 474–482.

Nakaya, U., 1954: *Snow Crystals*. Harvard University Press, 510 pp.

Nelson, L. D., 1979: Observations and numerical simulations of precipitation mechanisms in natural and seeded convective clouds. Ph.D. dissertation, University of Chicago, 188 pp.

Orville, H. D., and J-M. Chen, 1982: Effects of cloud seeding, latent heat of fusion, and condensate loading on cloud dynamics and precipitation evolution: a numerical study. *J. Atmos. Sci.* **39**, 2807–2827.

——, and F. J. Kopp, 1977: Numerical simulation of the history of a hailstorm. *J. Atmos. Sci.*, **34**, 1596–1618.

Passarelli, R. E., Jr., 1978: Theoretical and observational study of snow size spectra and snowflake aggregation efficiencies. *J. Atmos. Sci.*, **35**, 882–889.

Pflaum, J. C., and H. R. Pruppacher, 1979: A wind tunnel investigation of the growth of graupel initiated from frozen drops. *J. Atmos. Sci.*, **36**, 680–689.

Pruppacher, H. R., and J. D. Klett, 1978: *Microphysics of Clouds and Precipitation*. D. Reidel, 714 pp.

Rasmussen, R., and H. R. Pruppacher, 1982: A wind tunnel and theoretical study of the melting behavior of atmospheric ice particles. I. A wind tunnel study of frozen drops of radius < 500 μm. *J. Atmos. Sci.*, **39**, 152–158.

Rognlie, D. M., and F. J. Kopp, 1976: Application of direct Poisson solvers to time-dependent numerical cloud models. *Mon. Wea. Rev.*, **104**, 953–960.

Saunders, P. M., 1957: The thermodynamics of saturated air: a contribution to the classical theory. *Quart. J. Roy. Meteor. Soc.*, **83**, 342–350.

Strivastava, R. C., 1967: A study of the effects of precipitation on cumulus dynamics. *J. Atmos. Sci.*, **24**, 36–45.

Swarztrauber, P., and P. Sweet, 1975: Efficient Fortran subprograms for the solution of elliptic partial differential equations. NCAR-TN/IA-109, 139 pp.

Vali, G., 1971: Freezing nucleus content of hail and rain in Alberta. *J. Appl. Meteor.*, **10**, 73–78.

Wegener, A., 1911: *Thermodynamik der Atmosphäre*. Leipzig, J. A. Barth. 331 pp.

Wisner, C., H. D. Orville and C. Myers, 1972: A numerical model of a hail-bearing cloud. *J. Atmos. Sci.*, **29**, 1160–1181.

APPENDIX

List of Symbols

Notation	Description	Value	Units
a	constant in empirical formula for U_R	2115	$\text{cm}^{1-b}\ \text{s}^{-1}$
a_1	parameter in Bergeron process		$\text{g}^{1-a_2}\ \text{s}^{-1}$
a_2	parameter in Bergeron process		
A'	constant in Bigg freezing	0.66	K^{-1}
A''	coefficient in the diffusion equation for an ice particle		cm s g^{-1}
b	constant in empirical formula for U_R	0.8	
B'	constant in raindrop freezing equation	100	$\text{m}^{-3}\ \text{s}^{-1}$
B''	coefficient in the diffusion equation for an ice particle		cm s g^{-1}
c	constant in empirical formula for U_S	152.93	$\text{cm}^{1-d}\ \text{s}^{-1}$
C_D	drag coefficients for hailstone	0.6	
C_i	specific heat of ice	2.093×10^3	$\text{J kg}^{-1}\ \text{K}^{-1}$
C_p	specific heat of air at constant pressure	1.005×10^3	$\text{J kg}^{-1}\ \text{K}^{-1}$
C_w	specific heat of water	4.187×10^3	$\text{J kg}^{-1}\ \text{K}^{-1}$
d	constant in empirical formula for U_S	0.25	
D_0	dispersion of cloud droplet distribution	0.15	
D_G	diameter of hailstone		cm
D_R	diameter of a raindrop		cm
D_S	diameter of snow crystal		cm
E_{IW}	collection efficiency of cloud ice for cloud water	1	
E_{GI}	collection efficiency of hail for cloud ice	.1	
E_{GR}	collection efficiency of hail for rain	1	
E_{GS}	collection efficiency of hail for snow		
E_{GW}	collection efficiency of hail for cloud water	1	

APPENDIX (*Continued*)

Notation	Description	Value	Units
E_{RI}	collection efficiency of rain for cloud ice	1	
E_{SI}	collection efficiency of snow for cloud ice		
E_{SR}	collection efficiency of snow for rain	1	
E_{SW}	collection efficiency of snow for cloud water	1	
g	gravitational accleration	980.5	cm s^{-2}
K_a	thermal conductivity of air		J m^{-1} s^{-1} K^{-1}
K_h	heat eddy coefficient		cm^2 s^{-1}
K_m	momentum eddy coefficient		cm^2 s^{-1}
l_{CI}	mixing ratio of cloud ice		g g^{-1}
l_{CW}	mixing ratio of cloud water		g g^{-1}
l_G	mixing ratio of hail		g g^{-1}
l_{I0}	mass threshold for cloud ice aggregation	10^{-3}	g g^{-1}
l_R	mixing ratio of rain		g g^{-1}
l_S	mixing ratio of snow		g g^{-1}
l_{S0}	mass threshold for snow aggregation	6×10^{-4}	g g^{-1}
l_{W0}	mass threshold for cloud water coalescence used in P_{RAUT}	2×10^{-3}	g g^{-1}
L_v	latent heat of vaporization	2.5×10^6	J kg^{-1}
L_f	latent heat of fusion	3.336×10^5	J kg^{-1}
L_s	latent heat of sublimation	2.8336×10^6	J kg^{-1}
m_{I50}	mass of a 50 μm size ice crystal	4.80×10^{-7}	g
M_i	mass of one cloud ice crystal	4.19×10^{-10}	g
n_0	parameter in Fletcher's equation	10^{-8}	m^{-3}
n_{0G}	intercept parameters of hailstone size distribution	0.0004	cm^{-4}
n_{0S}	intercept parameter of the snowflake size distribution	0.03	cm^{-4}
n_{0R}	intercept parameter of the raindrop size distribution	0.08	cm^{-4}
N_1	number concentration of cloud droplets	1000	cm^{-3}
N_{I50}	number concentration of hypothetical 50 μm size ice crystal		g^{-1}
N_n	number of active natural ice nuclei		m^{-3}
P_G	total production rate of hail		g g^{-1} s^{-1}
P_S	total production rate of snow		g g^{-1} s^{-1}
P_R	total production rate of rain		g g^{-1} s^{-1}
P_{IMLT}	production rate for melting of cloud ice to form cloud water		g g^{-1} s^{-1}
P_{IDW}	production rate for depositional growth of cloud ice at expense of cloud water		g g^{-1} s^{-1}
P_{IHOM}	production rate for homogeneous freezing of cloud water to form cloud ice		g g^{-1} s^{-1}
P_{IACR}	production rate for accretion of rain by cloud ice		g g^{-1} s^{-1}
P_{RACI}	production rate for accretion of cloud ice by rain		g g^{-1} s^{-1}
P_{RAUT}	production rate for autoconversion of cloud water to form rain		g g^{-1} s^{-1}
P_{RACW}	production rate for accretion of cloud water by rain		g g^{-1} s^{-1}
P_{REVP}	production rate for rain evaporation		g g^{-1} s^{-1}
P_{RACS}	production rate for accretion of snow by rain		g g^{-1} s^{-1}
P_{SACW}	production rate for accretion of cloud water by snow		g g^{-1} s^{-1}
P_{SACR}	production rate for accretion of rain by snow		g g^{-1} s^{-1}
P_{SACI}	production rate for accretion of cloud ice by snow		g g^{-1} s^{-1}
P_{SAUT}	production rate for autoconversion of cloud ice to form snow		g g^{-1} s^{-1}
P_{SFW}	production rate for Bergeron process-transfer of cloud water to form snow		g g^{-1} s^{-1}
P_{SFI}	production rate for Bergeron process embryos (cloud ice) used to calculate transfer rate of cloud ice to snow		g g^{-1} s^{-1}

APPENDIX (*Continued*)

Notation	Description	Value	Units
P_{SDEP}	production rate for depositional growth of snow		g g^{-1} s^{-1}
P_{SSUB}	production rate for sublimation of snow		g g^{-1} s^{-1}
P_{SMLT}	production rate for snow melting to form rain		g g^{-1} s^{-1}
P_{GAUT}	production rate for autoconversion of snow to form graupel		g g^{-1} s^{-1}
P_{GFR}	probabilistic freezing of rain to form graupel		g g^{-1} s^{-1}
P_{GACW}	production rate for accretion of cloud water by graupel		g g^{-1} s^{-1}
P_{GACI}	production rate for accretion of cloud ice by graupel		g g^{-1} s^{-1}
P_{GACR}	production rate for accretion of rain by graupel		g g^{-1} s^{-1}
P_{GACS}	production rate for accretion of snow by graupel		g g^{-1} s^{-1}
P_{GSUB}	production rate for graupel sublimation		g g^{-1} s^{-1}
P_{GMLT}	production rate for graupel melting to form rain, $T \geq T_0$. (In this regime, P_{GACW} is assumed to be shed as rain.)		g g^{-1} s^{-1}
P_{GWET}	wet growth of graupel; may involve P_{GACS} and P_{GACI} and must include P_{GACW} or P_{GACR}, or both (The amount of P_{GACW} which is not able to freeze is shed to rain.)		g g^{-1} s^{-1}
P_{GDRY}	dry growth of graupel; involves P_{GACS}, P_{GACI}, P_{GACW} and P_{GACR}		g g^{-1} s^{-1}
q	mixing ratio of water vapor, cloud water, and cloud ice		g g^{-1}
r	mixing ratio of water vapor		g g^{-1}
r_s	saturation mixing ratio for water vapor with respect to water		g g^{-1}
r_{s0}	saturation mixing ratio for water vapor at surface of hail		g g^{-1}
r_{si}	saturation mixing ratio for water vapor with respect to ice		g g^{-1}
Δr_s	water vapor mixing ratio difference between saturation for hail and the environment $[=r_{s0} - r]$		g g^{-1}
R_{I50}	radius of hypothetical ice crystal	5×10^{-3}	cm
R_w	specific gas constant for water vapor	461.5	J kg^{-1} K^{-1}
S	saturation ratio		
S_c	Schmidt number $[=\nu/\psi]$		
S_i	saturation ratio over ice		
Δt_1	temperature dependent time scale		s
T	in-cloud temperature		K
T_0	melting temperature	273.15	K
T_{00}	reference temperature		K
T_c	temperature degrees Celsius		C
u	horizontal velocity		cm s^{-1}
U_G	mass-weighted mean terminal velocity of hailstones		cm s^{-1}
U_R	mass-weighted mean terminal velocity of raindrops		cm s^{-1}
U_S	mass-weighted mean terminal velocity of snowflakes		cm s^{-1}
U_{DG}	terminal velocity for hail of diameter D_G		cm s^{-1}
U_{DR}	terminal velocity for rain of diameter D_R		cm s^{-1}
U_{DS}	terminal velocity for snow of diameter D_S		cm s^{-1}
U_{I50}	terminal velocity of hypothetical ice crystal	100	cm s^{-1}
$\mathbf{V}$	vector notation of velocity		cm s^{-1}
w	vertical velocity		cm s^{-1}
α_1	autoconversion rate coefficient for P_{SAUT}		s^{-1}
α_2	autoconversion rate coefficient for P_{GAUT}		s^{-1}
β	parameter in Fletcher's equation	0.5	K^{-1}
δ_1	indicator for condensation (deposition) and evaporation (sublimation)		
δ_2	indicator of P_{RACS} and P_{SACR}		
δ_3	indicator of P_{IACR} and P_{RACI}		
θ	potential temperature		K
θ'	potential temperature deviation		K

APPENDIX (*Continued*)

Notation	Description	Value	Units
Θ	reference potential temperature		K
λ_R	slope parameter in rain size distribution		cm^{-1}
λ_S	slope parameter in snow size distribution		cm^{-1}
λ_G	slope parameter in hail size distribution		cm^{-1}
ρ_0	surface air density		$g\ cm^{-3}$
ρ	air density		$g\ cm^{-3}$
ρ_G	density of hail	0.917	$g\ cm^{-3}$
ρ_S	density of snow	0.1	$g\ cm^{-3}$
ρ_W	density of water	1	$g\ cm^{-3}$
ν	kinematic viscosity of air		$cm^2\ s^{-1}$
ψ	diffusivity of water vapor in air		$cm^2\ s^{-1}$
ϕ'	related to entropy		